A Hybrid Framework for Rapidly Locating Transition Zones: a Comparison of Event- and Response-based Return Water Levels in the Suwannee River FL

R. A. Jane[1], V. Malagón-Santos[1,2], M. M. Rashid[1,3], L. Doebele[1], T. Wahl[1], S. R. Timmers[4], K. A. Serafin[4], L. Schmied[5] and C. Lindemer[5]

[1]Civil, Environmental and Construction Engineering & National Center for Integrated Coastal Research, University of Central Florida, 12800 Pegasus Drive, Orlando, FL 32816, USA.

[2]Department of Estuarine and Delta Systems, NIOZ Royal Netherlands Institute for Sea Research, P.O. Box 140, 4400 AC, Yerseke, Netherlands.

[3]Global Science, The Nature Conservancy, 4245 North Fairfax Drive, Suite 100, Arlington, VA 22203-1606, USA

[4]Department of Geography, University of Florida, 330 Newell Dr., Gainesville, FL 32611, USA.

[5]Federal Emergency Management Agency. 500 C St., SW Washington, DC 20472, USA.

Corresponding author: Robert A. Jane (r.jane@ucf.edu)

Key Points:

- Transition zone of the Suwannee River, FL is approximately 45 km long and shifts depending on event frequency.
- Return levels associated with the "most-likely" design event closely match the response-based return levels for most of the transition zone.
- Scatter interpolation outperforms multiple linear regression and radial basis functions as a surrogate for the computationally expensive hydraulic model.

Abstract

Flood risk assessments commonly use event-based approaches to reduce the number of scenarios required to be run through computationally intensive physical process models. Often the return period of the response variable (e.g., a fluvial water level or overtopping discharge) generated by an event (e.g., upstream/downstream water level or set of sea state variables) does not match that of the event itself; a limitation of event-based approaches which can lead to the misspecification of flood risk. We present a transferable hybrid statistical - hydraulic modeling framework for rapidly locating transition zones; river reaches where extreme water levels are driven by both upstream riverine discharge and downstream sea level. Instead of an event-based approach the framework utilizes a surrogate model to reduce computational expense of the hydraulic model. The surrogate-based approach allows the empirical estimation of response-based along-river return levels from on a large number of plausible discharge – coastal still water level events simulated from the statistical model. We assess the robustness of the event-based approach by comparing the associated return levels with the response-based return levels. The framework is applied to the Suwannee River in Florida (United States). Three surrogate models are evaluated, highlighting the enhanced ability of non-linear models to accurately capture discharge-sea level interactions along the river. The along-river return levels of the "most-likely" design event is found to lie within the range of variability of the response-based return levels for most of the transition zone.

Plain Language Summary

Transition zones are stretches of river where the water level is driven by upstream river flow and downstream sea level. Techniques for evaluating flood risk in coastal rivers commonly model a single or small number of flow - sea level combinations that represent rare flooding scenarios, e.g., the flood event expected on average, once every 100 years. In transition zones, many different flow - sea level combinations can generate flooding consequently the 100-year flood generated from a single or few combinations may not represent the true 100-year flood. We develop a framework linking a statistical model with a river flow model to locate transition zones. Thousands of plausible flow - sea level combinations are simulated from the statistical model with their dependence preserved. Estimating along-river levels by running these combinations through a river flow model takes a very long time, thus we develop a proxy for the flow model. The transition zone is located by comparing combinations driving the 100-year water level with the upstream river flow and sea level expected with the same frequency. At our case study site, we find the 100-year water level extracted from our framework differ from those produced by existing techniques thus the latter may need to be reconsidered.

1 Introduction

Transition zones are stretches of river where extreme water levels can arise through the interaction of multiple drivers such as elevated river discharge, storm surge, and high tide (Bilskie and Hagen, 2018). Transition zones are likely to exist along rivers throughout the world and tend to be most dramatically revealed during catastrophic flood events, such as Hurricane Harvey (2017) where coincident heavy rainfall and surge flooded Houston and the surrounding area (Valle-Levinson et al., 2020). Storm surge and the rainfall that produces the elevated river discharge, are often generated by common synoptic conditions (Pfahl and Wernli, 2012), and are statistically dependent (e.g., Wahl et al. 2015; Nasr et al., 2021). Hydraulic modeling has shown discharge and surge often interact nonlinearly (Bilskie and Hagen, 2018), exacerbating the

impact of a flood to a greater (Kumbier et al., 2018; Silva-Araya et al., 2018; Gori et al., 2020) or lesser degree (Torres et al., 2015). Hence combining independently derived fluvial and coastal flood maps, as is currently being implemented for example by the U.S. Federal Emergency Management Agency (FEMA) as part of the National Flood Insurance Program, will likely mischaracterize the true flood risk (Bass and Obedient, 2018; Moftakhari et al., 2019).

Hydraulic models such as the Hydrologic Engineering Center- River Analysis System (HEC-RAS) (HEC, 2002) provide robust estimates of along-river water levels at the catchment scale (Loveland et al., 2021). Larger scale oceanic processes such as the wind driven storm surge can be accounted for implicitly in hydraulic models through boundary conditions, typically by coupling the hydraulic models dynamically or, more commonly, through a one-way coupling with a storm surge model (Santiago Cabello et al., 2019). For six historical landfalling tropical cyclones in North Carolina, Gori et al. (2020) identified two compounding mechanisms by loosely coupling HEC-RAS with a rainfall-runoff model at the upstream boundary and the ADcanced CIRCulation (ADCIRC) storm surge model at the downstream boundary. Moftakhari et al. (2019) and Serafin et al. (2019) developed hybrid frameworks, combining statistical modeling of the joint probabilities of the drivers with hydraulic models, to assess the compound flood hazard in transition zones. In the hybrid frameworks boundary conditions to date have taken the form of synthetic events generated from the statistical models. For example, in Serafin et al. (2019) long synthetic river discharge and coastal still water level time series act as boundary conditions for a HEC-RAS model of the Quillayute River in Washington State.

Despite increases in computational resources, propagating many scenarios through physics-based models often remains impractical (e.g., Robinson et al., 2008). One solution for limiting the computational cost is to combine a low fidelity numerical model, for example, a one-dimensional steady state model, with a relatively short record of synthetic conditions (e.g., Couasnon et al., 2018); however, this can lead to large uncertainties. Certain hybrid frameworks that attempt to estimate the flood hazard in transition zones (e.g., Moftakhari et al., 2019; Muñoz et al., 2020) and at the coast (e.g., Didier et al., 2019) adopt event-based statistical approaches to reduce the number of numerical model runs. Event-based approaches assume the response variable, in this case along-river water levels, are produced by the combination of the drivers with the equivalent return period (e.g., a certain combination of coastal water level and discharge with a bivariate return period of 50 years is assumed to lead to a 50-year water level along the river). Due to the physical interaction of the drivers, in reality, this will likely seldom be the case (e.g., Serinaldi, 2015). Generally, the event on a joint return period curve (or isoline) deemed "most-likely" according to the observational data is taken to represent the bivariate return period. The event-based approach combined with the "most-likely" strategy has the practical advantage of only requiring a single scenario per return period to be run through the numerical model. However, even assuming an exact correspondence between the return period of the drivers and response, using a single design event prevents a full characterization of the along-river levels associated with a bivariate return period. For instance, the "most-likely" event may not be the return level event that elicits the most extreme response (Lan et al. 2022), here the event that produces the highest along-river levels, potentially leading to under design and under estimation of flood risk.

In this context, surrogate models offer an alternative solution (Robinson et al., 2008). Surrogate models (also referred to as "response surfaces" or "meta-models") are essentially computationally efficient approximations of the deterministic physics-based models (Sacks et al.,

1989). The physics-based model is run for a subset of carefully chosen inputs while the responses of the remaining inputs are estimated by a surrogate model fit to these model runs. Data-driven surrogate models empirically approximate the relationship between the inputs (and parameters) and the outputs of a complex model without attempting to emulate any of its internal parts (Razavi et al., 2012). Past applications of surrogate models in fluvial and coastal flooding studies range from conceptually simple look-up tables (Apel et al., 2008) and empirical formulations (van Ormondt et al., 2021) to more complex approaches including Gaussian process models (Malde et al., 2016; Parker et al. 2019), kriging (Parker et al., 2019; Rohmer and Idier 2012), 3D scatter interpolation (Serafin et al., 2019), bilinear interpolation (Couasnon et al., 2022), radial basis functions (Camus et al., 2011a; Gouldby et al., 2014; Medellín et al., 2016; Rueda et al., 2016), support vector regression (Bermúdez et al. 2019; Chen et al. 2020; Jhong et al. 2017), random forests (Zahura et al. 2020), and artificial neural networks (Bermúdez et al., 2018; Peters et al., 2006; Santos et al., 2019). In a flooding context, the performance of the different models have rarely been compared. An exception is Bass and Bedient (2018), where kriging was shown to be a better surrogate than artificial neural networks for a 2D hydrodynamic model loosely coupled with a lumped hydrologic-hydraulic model forecasting peak inundation from tropical cyclones in Houston, Texas.

The predictive skill of the surrogate model will at least in part depend on the subset of inputs run through the physical models. The Maximum Dissimilarity Algorithm (MDA) (Kennard and Stone, 1969; Willett, 1999) aims to optimize surrogate model performance by identifying a user-specified sized subset of data that is most representative of the diversity of the underlying dataset. Camus et al. (2011b) found the MDA better represented the boundaries of a dataset (which are often the conditions leading to the most extreme responses) than other clustering techniques. Surrogate models aided by the MDA have been successfully developed for physics-based models of dune erosion (Santos et al., 2019), wave transformation (Gouldby et al., 2014; Molde et al., 2016; Rueda et al., 2016), wave run-up (Medellín et al., 2016), flood inundation (Bermúdez et al., 2018) and fluid-structure interactions (Lara et al., 2019).

The hybrid frameworks demonstrate that in the transition zones extreme water levels can be produced by individual discharge and coastal still water levels that are far less severe. Adopting a surrogate model enabled Serafin et al. (2019) to estimating along-river water levels for a long synthetic record of events, and in turn calculate response-based return levels empirically along the river. The authors demonstrated the disparity in the event-based return levels, i.e. water level given by the associated forcing event, under the assumption of full dependence between the forcings, and the response-based return levels for a range of return periods. The disparity may arise at least in part due to the assumption of full dependence leading to conservative event-based return periods. A natural next step is to investigate whether the disparity persists between the event-based and empirical response-based return levels, once the dependence between the forcings is accounted for in the derivation of the event-based scenarios, such as in Moftakhari et al. (2019). Comparing water levels generated by the “most-likely” design event with those produced by an ensemble of possible design events sampled along the same isoline will provide a preliminary assessment of the robustness of the “most likely” strategy.

The aim of this paper is twofold. Firstly, to develop a flexible hybrid statistical-numerical modeling framework for rapidly identifying transition zones, which is transferable and expandable. Secondly, to use the response-based return levels generated in finding the transition

zone to evaluate the robustness of the widely used event-based approach. The framework is implemented for the Suwannee River in northwest Florida representing the first application of such a framework to a river on the eastern U.S. coast. The first objective is to derive a long synthetic set of river discharge and coastal still water level events by fitting a statistical model that accounts for the dependence between the two flooding drivers. The second objective is to validate an existing HEC-RAS model for the case study site, through which an MDA-selected subset of synthetic events will be propagated. The third objective is to find a suitable data driven surrogate for the HEC-RAS model by evaluating the performance of several candidate models. Synthetic events not in the MDA subset will be propagated through the optimal surrogate model to obtain along-river water levels. The fourth and final objective is to compute response- and event-based return levels. Contrasting the individual components of the discharge and still water level events that produce a given return level along the river enables the identification of the transition zone. Comparing the along-river response- and event-based return levels will elucidate on the robustness of the event-based approach.

2 Case study site and data

The Suwannee River flows for around 396 km, with an average slope of 0.075 m per km (Valle-Levinson, 2012), and discharges into the Gulf of Mexico in northwest Florida. Described as a blackwater river, due to its stained hue caused by the tannic acids released by decaying vegetation that seep into its waters, the Suwannee is one of a few major rivers (>200 km in length) in the contiguous U.S. without any significant physical alterations such as dams, flow diversions, or navigation projects (Benke et al., 1990). The river drains an area of approximately 25,770 km^2, almost two thirds of which are in South Georgia and the remainder in North Florida (SRWMD, 2005). These larger catchments (>5,000 km^2) are generally less vulnerable to compound events than their smaller peers (Bevacqua et al., 2020). However, Dykstra and Dzwonkowski (2021) show that compound events are a more substantial issue for larger catchments in the northeastern Gulf of Mexico than previously believed, due to precipitation intensification shortening precipitation-discharge lag times.

The Suwannee River is fed by surface runoff from swamps, flatwoods, and lakes near its headwaters in the poorly drained tannic and black Okefenokee Swamp (South Georgia) in the eastern part of the Suwannee watershed (Katz et al., 1997). Upstream, the river initially flows southwest, merging with the Apalaha (highlighted in yellow in Figure 1a), and then the Withlacoochee River (orange in Figure 1a) 13 km farther downstream. The dendritic Apalaha and Withlacoochee Rivers drain the central and eastern portions of the Suwannee Watershed, respectively. The river channel deepens on its way south, as it bends southward joining with the Santa Fe River (green in Figure 1a), which drains much of the western portion of the watershed. The Suwannee continues on a south-southwest moderately sinuous course, increasingly restrained within a bedrock-lined channel, eventually flowing into the Gulf of Mexico in the Big Bend region of Florida's Gulf Coast (Mossa and Konwinski, 1998). The lower Suwannee Basin (Figure 1b) is a sparsely populated area dominated by poorly drained bottomland hardwood swamps, with silviculture and minor agriculture as the main land uses (Liudahl et al., 2005). The Suwannee estuary extends approximately 16 km upstream from where it drains into the Gulf of Mexico (Valle-Levinson, 2012).

Data used in this work consists of in situ observations of the still water level (SWL) at the coast and river discharge (Q) in the lower Suwannee. SWL represents the oceanographic forcing,

i.e., the downstream boundary condition in the HEC-RAS model, while Q acts as the freshwater forcing, i.e., the upstream boundary condition.

Hourly SWLs are obtained from the National Oceanographic and Atmospheric Administration (NOAA) (https://tidesandcurrents.noaa.gov/) for the tide gauge closest to the mouth of the Suwannee: Cedar Key (Figure 1a). The gauge has 94 years of record (not all years are complete), from three distinct periods: 1914 to 1926, 1932 to 1934, and 1938 to 2020 (Figure 1c). The SWL is composed of the mean sea level (MSL) relative to a datum, astronomical tide, and the non-tidal residual (NTR). The NTR is primarily composed of the meteorologically driven surge, along with the seasonal cycle and monthly mean sea level anomalies. Other influences include precipitation, river discharge, nonlinear interaction with the tide and harmonic prediction errors emanating from the process of removing the tidal signal (Haigh et al., 2016). The SWL series is detrended to ensure stationarity, an inherent assumption of the statistical models introduced in Section 3.1. Here we use a linear regression and the resulting series is adjusted to present-day conditions by adding the MSL of the past five years (e.g., Nadal-Caraballo et al., 2016). The NTR is often small relative to tide, consequently significant correlation between the river discharge and surge can be lost if SWL is used to represent the oceanic forcing (e.g., Moftakahri et al., 2019). Hence, the tidal signal was removed from the SWL by conducting a harmonic analysis on the SWL record using the T_Tide Matlab Toolbox (Pawlowicz et al., 2002), and the daily maximum NTR were selected as input for the statistical analysis.

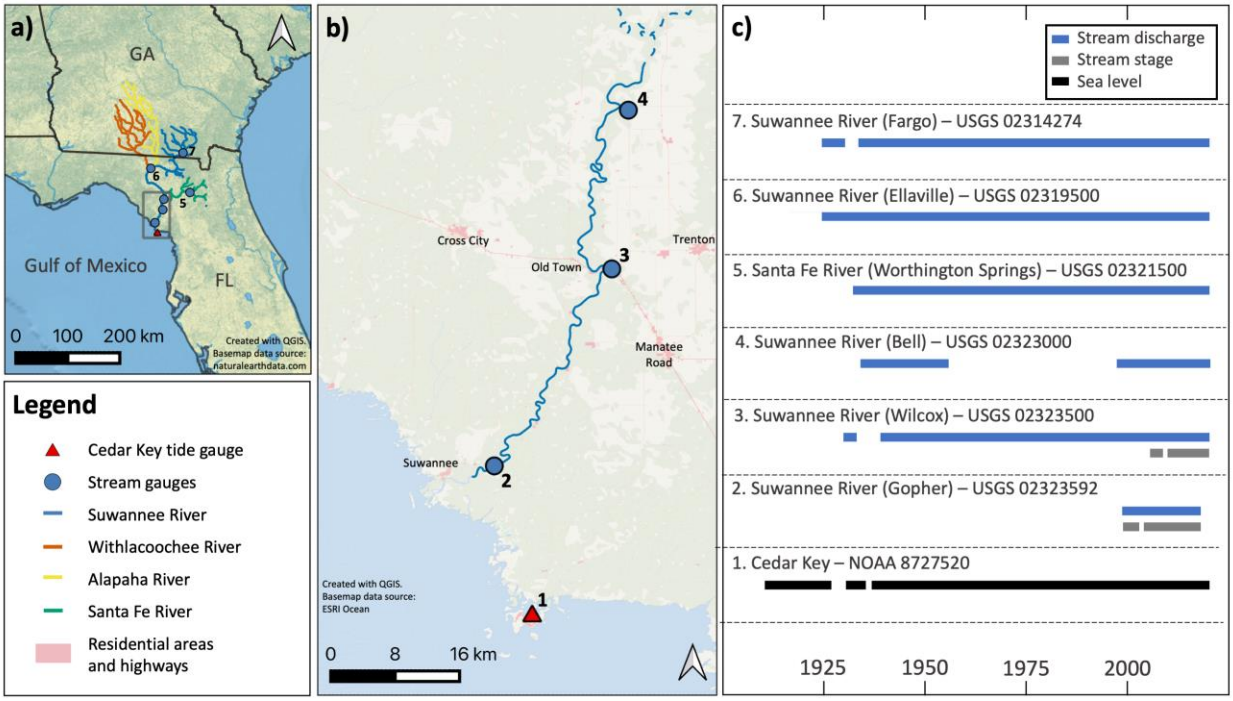

Figure 1: Case study site. (a) Location of tide and stream gauges in the Suwannee River and its main tributaries. (b) Grey box in (a), solid blue line denotes the HEC-RAS model. (c) Completeness of the observation records.

Daily mean Q data are obtained from the U.S. Geological Survey (USGS) stream gauge network (https://waterdata.usgs.gov/nwis/rt). We identified 40 USGS stream gauges along the Suwannee River and its tributaries, those with the longest record are shown in Figure 1a. Data availability for the longest records and those in the lower basin are shown in Figure 1c. The Bell

gauge, which has approximately 45 years of record from 1932 to 1956 and from 2000 to 2020, is adopted as the upstream boundary. Despite not possessing the longest record in the lower watershed, Bell is selected because it is downstream of all major tributaries. This, simplifies the numerical model set-up and at 105 km upstream, the Bell record is not unduly influenced by tides. Moreover, there are two gauges located downstream of Bell which provide an opportunity to validate the numerical model. The model validation is undertaken using the stage recorded at the Wilcox gauge which is located around 50 km upstream of the river mouth and spans 2007-present. Despite evidence of a falling annual discharge volume to annual basin rainfall ratio (Seavey et al., 2011), neither the Pettitt's change point test (Pettitt, 1979) nor the Mann-Kendall trend test (Kendall, 1975; Mann, 1945) were statistically significant at Bell. Since there is no evidence of non-stationarity, the discharge records were not detrended.

3 Methods

3.1 Hybrid statistical-hydraulic modeling framework

Hybrid approaches combining statistical and numerical models, that involve developing a surrogate model for the latter, have become increasingly prevalent over the past decade. The approach put forward in this paper proceeds by simulating boundary conditions from a statistical model fit to the observational records. A subset of the simulated conditions are run through a high-fidelity numerical model. A surrogate model is then fit to the input and output of the numerical model runs, before the remaining boundary conditions are propagated through the surrogate model. The precise form of the approach adopted in this paper is summarized in Figure 2. It closely resembles similar recent applications for estimating the compound flood hazard in coastal catchments by Parker et al. (2019) and Serafin et al. (2019). Each component of the method is described in more detail in the following subsections.

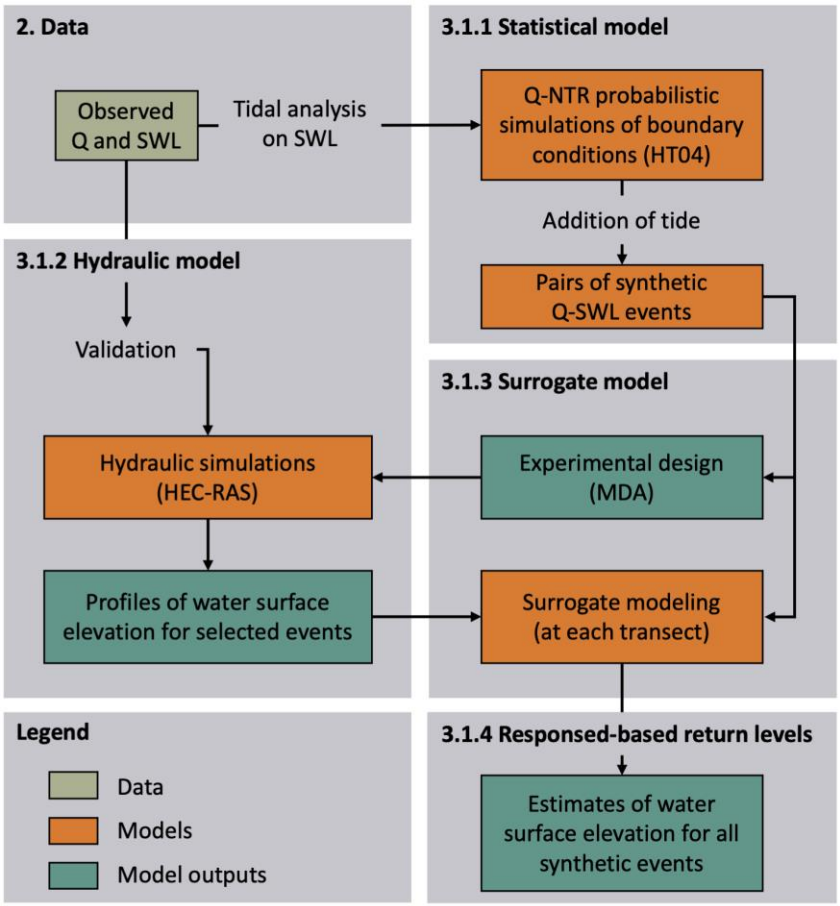

Figure 2: Hybrid modeling approach where numbering is aligned with section numbers of the main text where the respective part of the analysis is explained in detail. Tan boxes denote data inputs, orange boxes are the statistical, hydraulic and surrogate models while the green boxes correspond to the outputs from these models. MDA refers to the Maximum Dissimilarity Algorithm and HT04 to the conditional exceedance approach outlined in Heffernan and Tawn (2004).

3.1.1 Statistical model

We employ the conditional exceedance approach introduced in Heffernan and Tawn (2004) (hereinafter HT04) to simulate 10,000 years' worth of extreme daily synthetic Q - NTR events under present-day climate conditions that account for the dependence between the two drivers. The HT04 approach models the pairwise dependencies between the cluster maxima of a given variable above a sufficiently high threshold and the other variables, regardless of whether the latter are simultaneously extreme or not. A separate multivariate regression model is fit, as each variable is in turn conditioned to be extreme. The approach thus captures the dependence through the regression parameters and associated residuals rather than prescribing a specific dependence structure by way of a parametric distribution such as the logistic model or copulas. These earlier approaches assume the class of dependence in the joint tail regions is homogenous among each pair of variables, which becomes a restrictive assumption as more variables are considered. Recently, the HT04 model (Santos et al., 2021a) and other approaches such as Bayesian networks (Couasnon et al., 2018) or a cascade of bivariate copulas, so called pair

copula constructions (Bevacqua et al., 2017; Santos et al., 2021b) that remove this assumption have been employed to model the relationship between storm surge and river discharge at multiple sites in a catchment.

The HT04 approach decouples the modeling of the marginal characteristics and the dependence structure. The marginal behavior of each flooding driver is analyzed individually using the Peaks-Over-Threshold (POT) approach, where the peak excesses above a sufficiently high threshold are fit to a Generalized Pareto Distribution (GPD). For Q, we applied a 7-day storm window following previous studies of similar sized catchments (e.g., Santos et al., 2021a). NTR is declustered using the method described by Smith and Weissman (1994), where successive exceedances are assumed independent if the number of non-exceedance between them exceeds some separation criterion. Here a 3-day separation criterion was applied. To obtain a fully specified marginal distribution for driver X_i, the GPD above the threshold u_i is combined with the empirical distribution $\tilde{F}_i$ below the threshold, yielding the following semiparametric cumulative distribution function (Coles and Tawn, 1991):

$$\hat{F}_i(x) = \begin{cases} \tilde{F}_i(x) & x \leq u_i \\ 1 - (1 - \tilde{F}_i(u_i)) \left[1 + \frac{\xi_i (x - u_i)}{\beta_i}\right]_+^{-\frac{1}{\xi_i}} & x > u_i \end{cases}$$

Where, $\beta_i > 0$ and $\xi_i \in R$ are the GPD parameters and $[y]_+ = max(y, 0)$

In the dependence analysis, the variables are transformed to common scales to remove the marginal characteristics and ensure only information regarding the dependence structure remains. When implementing the HT04 approach, variables are typically converted to standard Gumbel marginal distributions obtained by setting $Y_i = -log\,[-log\,(F_i(X_i))]$. Letting $\boldsymbol{Y}_{-i}$ be the vector of all drivers excluding Y_i on the transformed scale, the HT04 model is generally implemented utilizing the multivariate non-linear regression model:

$$\boldsymbol{Y}_{-i}|Y_i = \boldsymbol{a}Y_i + Y_i^{\boldsymbol{b}}\boldsymbol{Z} \text{ for } Y_i > v$$

Where v is a high threshold on Y_i, $\boldsymbol{a} \in [0,1]$ and $\boldsymbol{b} < 1$ are parameters, and $\boldsymbol{Z}$ is a vector of residuals. Parameter estimation is carried out using maximum-likelihood estimation under the temporality assumption that $\boldsymbol{Z}$ follows a normal distribution with unknown mean and variance. Asymptotically, $Y_i > v$ is statistically independent of $\mathbf{Z}$, thus v should be large enough for this condition to hold. The number of simulated events, representing the 10,000 years' worth of extremes, depends on the average number of events in the observational record exceeding *v*. A detailed description of the rejection sampling methodology involving conditioning a variable to exceed *v* and independently sampling joint residuals to simulate extreme events is given in Keef et al. (2009) and Wyncoll and Gouldby (2015), among others.

The NTR and Q peaks that produce extreme along-river levels during a storm event may not occur concurrently. Keef et al. (2009) modified the HT04 approach to model the largest values within a time window, by fitting the regression model over a range of lags τ, i.e. to $\boldsymbol{Y}_{j,t+\tau}|\boldsymbol{Y}_i$. In this study, a lag of ± 1 day is adopted due to the relatively short distance between the upstream and downstream boundary conditions. In short, a variable is conditioned to exceed *v* and a joint residual from the associated regression model is independently sampled. The

maximum value of each of the remaining variables across the lags is found by plugging the residuals into the associated regression model. The realization is rejected if the conditioned variable is not the most extreme on the transformed scale. The sampling is repeated conditioning on each variable, in turn, to ensure the proportion of times each variable is most extreme is the same as the empirical data.

Once paired Q - NTR events are simulated from the model, a tidal level is obtained in accordance with Gouldby et al. (2014). For each simulated daily maximum NTR, we first sample a year in the 18.6-year nodal tidal cycle (Haigh et al., 2011). A month is then sampled conditionally on each simulated NTR: the conditional distribution of months given the percentile that a simulated NTR falls within (NTR_p) is shown in Figure 3. An hourly tidal elevation that co-occurred with a maximum hourly NTR in this year and month combination is sampled assuming the observations are equally likely. The sampled tidal level is added to the simulated NTR to give the SWL. The entire procedure yields 10,000 years' worth of simulations under present-day climate conditions based on the average number of events in the observational record.

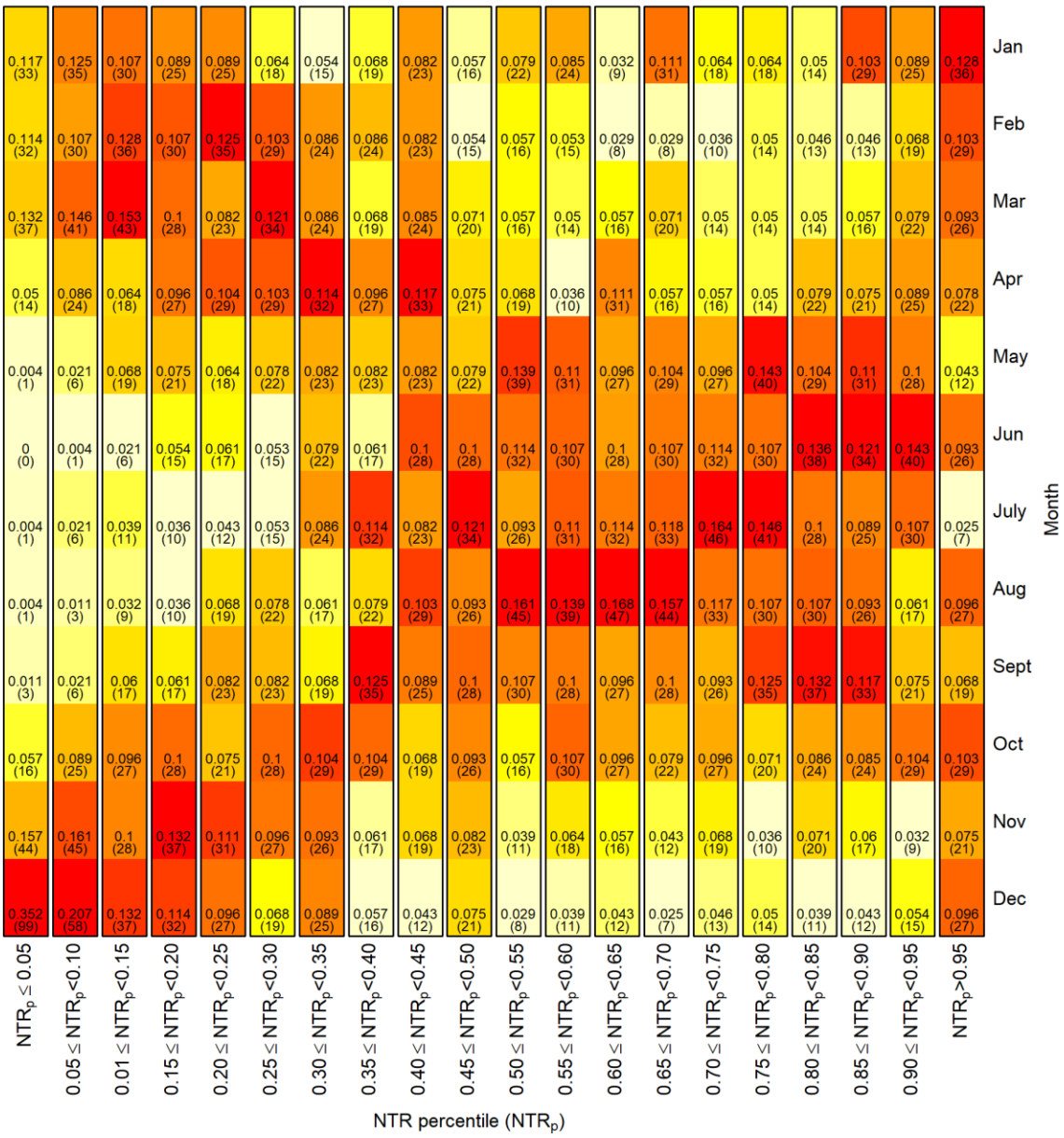

Figure 3: Conditional distribution of month given NTR percentile (NTR_p). Numbers without parenthesis are the conditional probabilities while the numbers in parenthesis denote the number of observed NTRs within each NTR_p – month combination. Color scale represents the conditional probabilities (hotter color, higher probability). For a simulated NTR, a month is sampled with probabilities depending on the NTR_pwithin which the NTR falls. Given an independently sampled year, an hourly tidal level that co-occurred with a daily maximum NTR is sampled assuming each level within the identified year-month combination is equally likely.

3.1.2 Hydraulic model

In 1D hydraulic modeling, a river's topography is described by a series of cross sections and the average velocity and water depth at each cross-section is estimated considering only longitudinal flow. The 1D form of the Hydrologic Engineering Center – River Analysis System

(HEC-RAS) model, developed by the U.S. Army Corps of Engineers, calculates water surface elevations by solving the one-dimensional energy equation from one cross section to the next using the standard step iterative procedure (HEC, 2002). HEC-RAS can model steady (constant discharge) and unsteady (varying discharge) flow under subcritical, supercritical and mixed flow regimes (Goodell, 2014). HEC-RAS models have proven sufficiently reliable (e.g. Andrei et al., 2017; Huţanu et al., 2020; Pathan and Agnihotri, 2020) for diverse applications ranging from flood forecasting (Hicks and Peacock, 2005; Saleh et al., 2017) to modeling dam breaches (Yi, 2011). In this work, we employ the 1D gradually varied steady-flow HEC-RAS model of the Suwannee River developed by AMEC Environment & Infrastructure, Inc. (AMEC) for the Suwannee River Water Management District (SRWMD) AMEC SRWMD (2013; 2014) for delineating flood insurance maps. The model was calibrated and validated using observational data and is publicly available from SRWMD (2014). The model covers the Suwannee River and its major tributaries. Here, the model is modified to only span the portion of the Suwannee River seaward of the Bell gauge which is around 10 km downstream of its confluence with the Santa Fe River, as highlighted in Figure 1a. The modified model is composed of 48 transects and is validated using water surface measurements from Wilcox (Figure 1c), as it possesses a longer record than the Gopher River gauge. The Cedar Key tide gauge is the downstream boundary of the model.

The HEC-RAS model validation was undertaken on 100 events selected via MDA from the Q- SWL observations, when stage height is concurrently available at the Wilcox gauge. The MDA is designed to select a subset that represents the diversity of the dataset (Camus et al., 2011b). After normalizing the input variables, the MDA algorithm proceeds by transferring a single element into a subset and iteratively adding the element remaining in the dataset that is most dissimilar, i.e., considered farthest in the multidimensional space from the elements already selected. Although each cluster based technique possesses distinct merits, e.g., self-organizing maps provide an opportunity for visual inference, the MDA is adopted here as it best represents the boundaries of the dataset (Camus et al., 2011b). A Root-Mean Squared Error (RMSE) of 0.1 m was obtained between the observed and modeled water levels at Wilcox for the 100 events. This small average discrepancy demonstrates the good performance of the model for a variety of events ranging from small, through moderate, to extreme (orange dots in Figure 4a). Since the Wilcox gauge is located where fluvial processes and the most extreme SWLs have the potential to drive water level variations, the validation conveys the suitability of the model to assess the compounding effects.

3.1.3 Surrogate model

The number of MDA-selected events to which surrogate models are fit is subjective, representing a trade-off between the computational cost of running the physics-based model and performance of the fitted surrogate model. The surrogate model performance achieved by an MDA sample size depends on the number and distribution of variables, type of surrogate model, and complexity of the physical process being modeled (Liem et al., 2015). In previous hydrologic applications, 100-200 MDA-selected events were typically found to provide sufficiently accurate surrogate models (e.g., Camus et al., 2011b; Malde et al., 2016). HEC-RAS is a relatively simple and efficient model compared to those utilized in similar studies, affording the opportunity for a larger MDA sample size. For example, Serafin et al. (2019) compared 3,000 surrogate modeled water levels with the corresponding HEC-RAS-modeled water levels as surrogate model validation.

We develop surrogate models for each transect using the along-river water level output of the validated HEC-RAS model for a subset of 1,000 boundary conditions (i.e., Q and SWL) from the large set of events simulated from the HT04 model. The surrogate models allow along-river water levels to be predicted for Q - SWL combinations while limiting the number of HEC-RAS simulations required. The subset of boundary conditions is selected using the MDA with the aim of optimizing the performance of the surrogate model, given the user-specified subset size. We consider three methods to develop surrogate models: multiple linear regression, radial basis function (Lin and Chen, 2004; Soleymani et al., 2016; Majdisova and Skala, 2017), and scattered interpolation (Amidror, 2002). The multiple linear regression model is conceptually the simplest but also possesses the most restrictive assumptions. The model comprises a constant intercept term, slope for each explanatory variable (expressing the change in the response with a one unit increase of the explanatory variable while holding all other variables constant) and a residual term. As the name suggests, a linear relationship is assumed between the response variable and each of the exploratory variables. The model also assumes the residuals are independent and normally distributed with a zero mean and constant variance across all values of the explanatory variables.

The interpolation function in the radial basis function model is a linear combination of radial basis functions, one centered on each observation. A radial function is any real valued function that decreases monotonically with distance from a central point. In this work, the radial basis function approximation takes the form of a weighted sum of Gaussian basis functions. Weights are estimated via the least mean square algorithm and shape parameters of the Gaussian basis functions, which controls their flatness, are estimated from sample data. In scatter interpolation, data points are triangulated (for 2D data) or tetrahedralized (for 3D data) and interpolation is carried out within each triangle (or tetrahedron) (Amidor et al., 2002). In this study, we deploy three interpolation techniques: linear, nearest, and natural (Boissonnat et al, 2002; Parker et al., 1983). As opposed to the multiple linear regression model, both the radial basis function and scatter interpolation models can capture nonlinear relationships between the response and exploratory variables.

The performance of each surrogate model at each transect is assessed through k-fold cross validations. In a k-fold cross validation, MDA selected events are divided into k-subsets, before each subset is used to validate the surrogate model fit to the remainder of the MDA events. For example, for k = 5, five subsets are created, each containing 200 events in our case, which are in turn used to validate the surrogate model fit to the events in the other four subsets. Varying the number of folds in the cross-validation undertaken on the surrogate models will provide a posteriori validation of the MDA sample size. Finally, the best performing surrogate model is used to predict water levels at each transect for the Q - SWL events simulated by the HT04 approach in Section 3.1.

3.1.4 Response-based return levels

The proposed framework returns 10,000 years' worth of extreme water levels at each transect of the HEC-RAS model, allowing response-based return levels to be estimated empirically. Response-based return levels represent a bottom-up approach where, the return period of the i^{th} highest water level at each transect is $\frac{\mu}{1-\hat{F}}$ years. Where μ is the average interarrival time between the N simulated events (in years) and $\hat{F} = \frac{i}{N+1}$ is the empirical

cumulative distribution function of water levels at the transect. The transition zone can subsequently be identified by analyzing individual Q - SWL events that produce the response-based return levels.

3.2 Comparing response- versus event-based return levels

In the event-based approach, along-river water levels produced by the Q - SWL design event associated with a given return period are assumed to be representative of this condition. Outside of the univariate domain, design events are not uniquely defined. To find design event(s) in the bivariate and higher-dimensional domains a hazard scenario (e.g. OR, AND, Kendall's, Survival Kendall's) must be prescribed alongside the return period. No hazard scenario is universally superior but each represents a different specific underlying probability. The choice of scenario should reflect the types of events considered most impactful; thus, the hazard scenario approach provides a top-down appraisal of the flood hazard (Serinaldi, 2015). The Kendall and survival Kendall hazard scenarios are most closely aligned with the univariate return period definition, however they do not have a direct physical interpretation. The Kendall scenarios are consequently generally only considered suitable for preliminary assessments of multivariate occurrence probabilities (Salvadori et al., 2016). This study focuses on events where both discharge and ocean still water level contribute to flooding. Therefore the "AND" scenario is adopted. This is also in line with similar recent studies assessing the flood hazard from two drivers in low-lying coastal catchments (e.g. Jane et al., 2022; Lucey et al., 2022; Moftakhari et al., 2019).

In the bivariate setting, the "AND" scenario yields an isoline, a curve comprising all events where the probability of both variables exceeding both thresholds corresponds to a specified joint return period. The "most-likely" approach is a simple strategy for identifying a single design event, by weighting the events on the isoline according to the joint distribution of the observations (Salvadori et al., 2011). The event on the isoline with the maximum probability density is taken as the design event, i.e., it may be considered the expected event if the return period arises. Uncertainty in design event selection is accounted for by sampling the probabilistically weighted events on the isoline to generate an ensemble of design events (Gräler et al., 2013). The interaction of multiple drivers typically distorts the mapping of the event-based return levels and the actual return water levels. The response-based return levels described here are assumed to be closer to the true return levels, as they are derived through a bottom-up approach utilizing a long, albeit synthetic, record rather than a top-down approach based on a single or small number of design events. Event-based return levels are compared with the response-based return levels to examine the robustness of the event-based approach. Comparing the event-based return levels from an ensemble rather than a single design event permits a more rigorous assessment.

4 Results

4.1 Application of the statistical-numerical hybrid model

Even weak extremal dependence can significantly influence flood hazard and thus must be accounted for in a robust framework (Zheng et al. 2014). Two-way conditional sampling was applied to the Q and NTR observations (Figure 4b) to gauge the strength of the dependence when each driver is extreme. In two-way conditional sampling, cluster maxima of one driver above the threshold are paired with the maximum value of the other variable within a specified lag. The

thresholds and lags are chosen to be consistent with those adopted in the HT04 model. Kendall's τ is 0.025 (p-value >0.05) for the sample conditioned on NTR, and -0.06 (p-value >0.05) for the sample conditioned on Q. The weak correlation in the sample conditioned on NTR is potentially caused by the catchment's gentle slope and plentiful storage capacity, delaying rainwater reaching the river. Moreover, Q accounts for groundwater contributions to the flow upstream of Bell, which varies over longer time scales than a single event, potentially further diluting the correlation. The synthetic simulations from the statistical model outlined in Section 3.1.1, comprising approximately 365,000 realizations representing 10,000 years of extreme events, are displayed in Figure 4c.

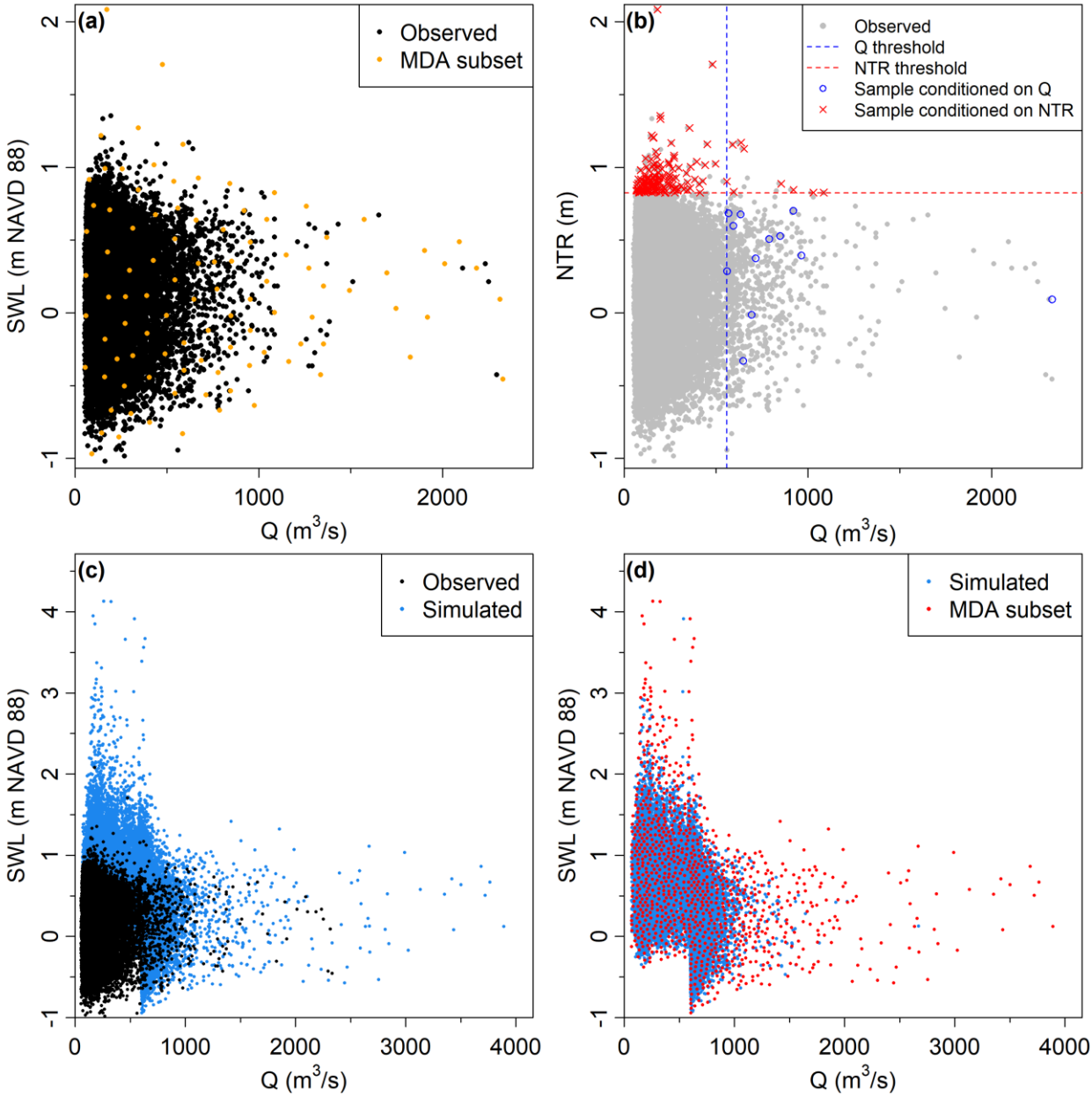

Figure 4: Data: (a) Observed Q-SWLs (black dots) delineating those chosen by the MDA (orange dots) for the HEC-RAS model validation. (b) Observed Q-NTRs (gray dots) along with the thresholds (blue and red dashed lines) above which the conditional samples (blue dots, red

crosses) are drawn and the HT04 model is fit. (c) Simulated events (blue dots) plotted alongside the observations (black dots) and (d) simulated events (blue dots) plotted identifying the events selected by the MDA (red dots) to run through the validated HEC-RAS model to which the surrogate models are fit. Nine simulated events are outside of the axis limits and are therefore not displayed. Q is the daily mean discharge and SWL is the sum of daily maximum hourly NTR and a conditionally sampled tidal level.

4.2 Comparison of surrogate models

The 1,000 simulated events selected by the MDA to be run through the HEC-RAS model are shown in Figure 4d. The performance of the three surrogate models at each transect, quantified in terms of the Root Mean Squared Error (RMSE) and normalized RMSE (NRMSE) from the k-fold cross-validations, are shown in Figure 5. As expected, the ability of each model to predict water levels improves with k, the number of folds (subsets) the MDA selected events are divided into, since the model is fit to more events. The rate of improvement wanes as k increases, since the number of additional observations the model is fit to dramatically decreases. In other words, the performance of the surrogate models is generally very similar for k = 5,10, 25, and 50. This trend suggests that k = 5 representing a subset of 800 events would give a sufficiently robust surrogate model, highlighting the suitability of a 1,000 sized MDA sample. All three models demonstrate good accuracy with average RMSEs in the order of centimeters. The ability of the multiple linear regression model to predict along-river levels steadily decreases (i.e. errors increase) with distance from the river mouth. Errors from the scatter interpolation and radial basis function models follow a similar spatial pattern, indicating that the models perform best near the mouth of the river and upstream; both regions where water levels are driven by a single driver. The cross-validation reveals scatter interpolation as the best surrogate model and it is thus adopted for the subsequent analysis.

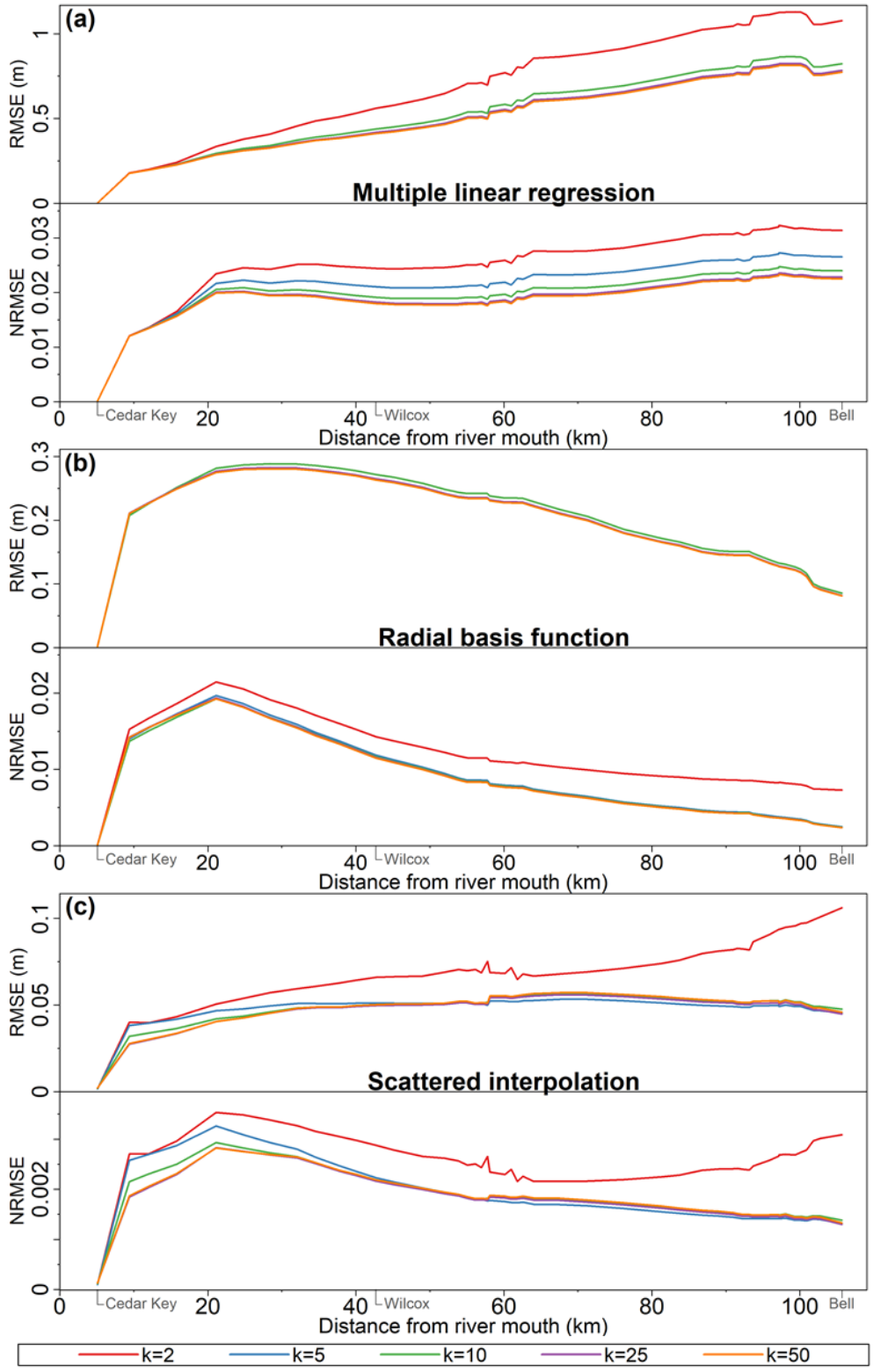

Figure 5: Performance of the surrogate models: (a) multiple linear regression, (b) radial basis function and (c) scattered interpolation during the k-fold cross-validations with varying values for k (2, 5, 10, 25, and 50). Note the varying scale of the y-axes.

4.3 Return levels

4.3.1 Delineation of the transition zone

Outside the transition zone, return levels are only produced by the corresponding marginal Q or SWL events, since water level is driven exclusively by discharge or coastal still water level. On the other hand, inside the transition zone a return level can be produced by the interaction of Q and SWL events with shorter marginal return periods. Comparing the individual components of the Q-SWL events that produce the along-river return water levels will hence allow the identification of the transition zone.

Figure 6 shows the average magnitude of Q (a) and SWL (b) conditions leading to the 5, 10, 25, and 100-year "response-based" return levels across the model domain. Few of the simulated events in the sample exactly replicate each "response-based" return period. The average magnitudes of Q and SWL are therefore calculated based on events with return periods within an interval centered on the return period of interest. The intervals for the 5, 10, 25 and 100-year return levels are: [4,6]; [8,12]; [20,30]; [80,120] years, respectively. Intervals widen as return period increases, as shorter return period (e.g., 5-year) events far outnumber those with longer (e.g., 100-year) return periods in the simulated sample. The magnitude of Q (solid lines in (a)) increases asymptotically for all return periods with distance from the river mouth. The increase in Q is steep until around km 25 and slower farther upstream. The average Q attains a value equivalent to the marginal Q return level (dashed lines in (a)) around km 55. The exception is the 100-year return level scenario, where the average Q reaches the corresponding marginal return level at river km 40. The average 100-year SWL (solid lines in (b)) almost immediately diverges from the marginal return level (dashed lines in (b)) while the magnitude of the other SWLs remain close to their corresponding marginal return periods until around km 10. The divergence in behavior between 100-year and other return periods suggests the transition zone shifts farther upstream for high frequency events while for low frequency events it is situated closer to the river mouth. The wider interval of the events considered for the average calculation of the 100-year event scenario (i.e. 80 to 120 years) compared to other return periods, to ensure a sufficient number of events are included in the calculation, may be a contributing factor behind this divergence.

As expected, the trend in the average SWLs (solid lines in (b)) mirrors the trend in average Q. The average SWLs associated with the shorter return levels decrease relatively uniformly with distance upstream. The 25- and 100-year return levels decrease rapidly until around km 40. The average SWL associated with the 100-year return level is negligible beyond km 40. By km 55, average SWLs are substantially lower than the marginal SWLs for all return levels. Based on these trends the transition zone of the Suwannee River approximately spans river km 10 to 55 but shifts towards the river mouth: km 5 to km 40 for low frequency events e.g., 100-year events. In both cases this is substantially longer than the 1 km zone estimated for the Quillayute River and the 0.6 to 2.1 km transition zones found for three rivers in Southern California in similar studies by Serafin et al. (2019) and Moftakhari et al. (2019), respectively. The substantially shallower slope of the Suwannee, at least compared to the Quillayute, is likely the main reason for a longer transition zone. Along the U.S West Coast, surge heights are also restricted by the narrow continental shelf, limiting the upstream reach of the ocean's influence.

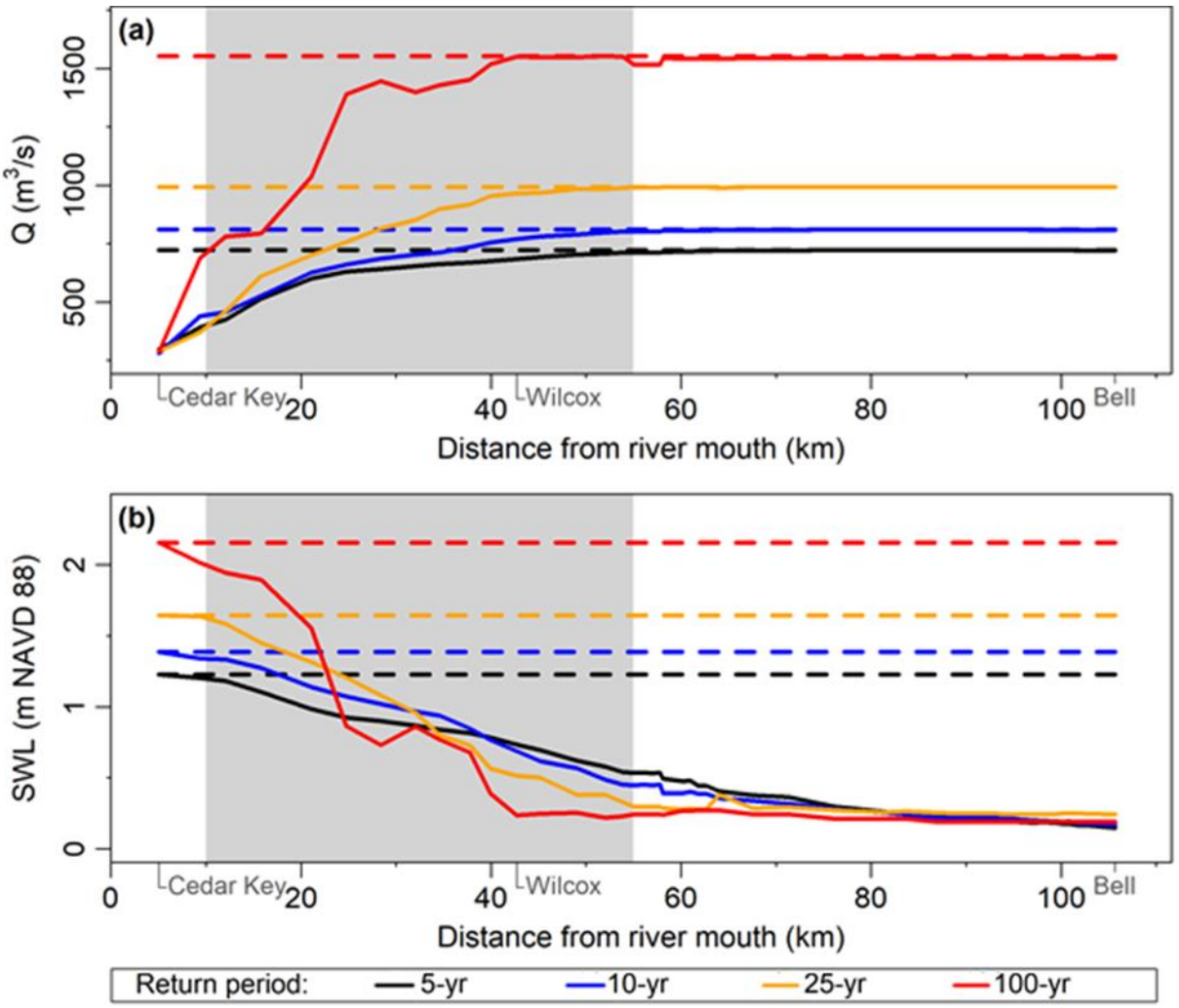

Figure 6: Solid lines are the average (a) Q and (b) SWL driving return water levels across the domain. Dashed lines represent marginal return period events. Gray shaded area depicts the transition zone.

4.3.2 Response- versus event-based return levels

Event-based along-river levels are derived for a 100-year return period by applying the conditional sampling-copula theory approach outlined in Jane et al. (2022) to the observations. The approach begins by drawing two conditional samples, similar to that described in Section 3.1.1 and modeling the dependence within each using the best fitting of 40 copulas. In terms of marginals distributions, the conditional variable is modeled by the GPD and the non-conditioned variable by the best fitting of a range of suitable e.g., truncated/non-truncated parametric distributions. The 100-year quantile isolines are subsequently derived for each sample. The full 100-year isoline comprises the outer envelope created by overlaying the (quantile) isolines from the two conditional samples (Bender et al., 2016). The 100-year isoline including the relative probability of events on the isoline implied by the observations is shown along with the "most-likely" design point and the ensemble of 1,000 possible design events in Figures 7a and 7b. The

probability density is concentrated on a portion of the isoline where the SWL is large relative to Q, hence there is a bias towards selecting these events.

Figure 7c depicts the estimated 100-year return levels from the response-based approach and an event-based approach adopting the "most-likely" strategy to select a single design event. The "most-likely" design event strategy results in consistently lower water levels than the response-based return levels. Initially the disparity between the "most-likely" and response-based return levels decreases with distance from the river mouth, with a minimum difference of 0.07 m at km 25. The disparity widens moving upstream reaching 0.4 m by the end of the transition zone, beyond which the difference in the two water levels remains constant. The smallest difference in the water levels arising closer to the seaward end of the transition zone is likely due to the 100-year "most-likely" design events being predominantly SWL driven (see Figure 7a). Despite this, the largest difference is at the river mouth where the response-based return levels exceed those given by the "most-likely" design event by over a meter. The joint statistical analysis (Figure 7a) suggests the 100-year SWL at the mouth is approximately 2.4 m NAVD 88 while the SWL in the "most-likely" design event is approximately 1.25 m NAVD 88. Given there is no fluvial influence on return levels at the mouth a difference of a little over a meter is to be expected.

Figure 7c also displays the distribution of the 100-year event-based return levels produced by an ensemble of 1,000 possible design events sampled along the 100-year isoline. The variation in the water levels among the ensemble runs increases with distance upstream, a seemingly intuitive result as the water level is increasingly only dependent upon Q which varies far more than SWL. The result is also consistent with output from the HEC-RAS model runs where there is more variation in output upriver than downriver, and is potentially due to the uncertainties associated with converting Q into water levels. The spread of the distribution demonstrates that the along-river water levels produced by events on the 100-year isoline can fall far above and far below the 100-year response-based return level. Design event selection thus requires careful consideration to avoid selecting event(s) that lead to under- or over-design. This disparity in the return levels demonstrates a known limitation of event-based approaches, as they do not account for 'structural performance', in other words there is a mismatch between the return periods of the response (here along-river water levels) and of the drivers (e.g., Serinaldi, 2015). Despite this, the "most-likely" event is situated close to the median of the return level distribution from the ensemble and, although consistently lower than the response-based return level, for most of the transition zone, the disparity is small. Hence, for our particular study site results in Figure 7c justify employing the "most-likely" design event strategy within most of the transition zone. In flat floodplains, however, small changes in water level can result in significant changes in flood extent, thus the strategy should still be applied with caution.

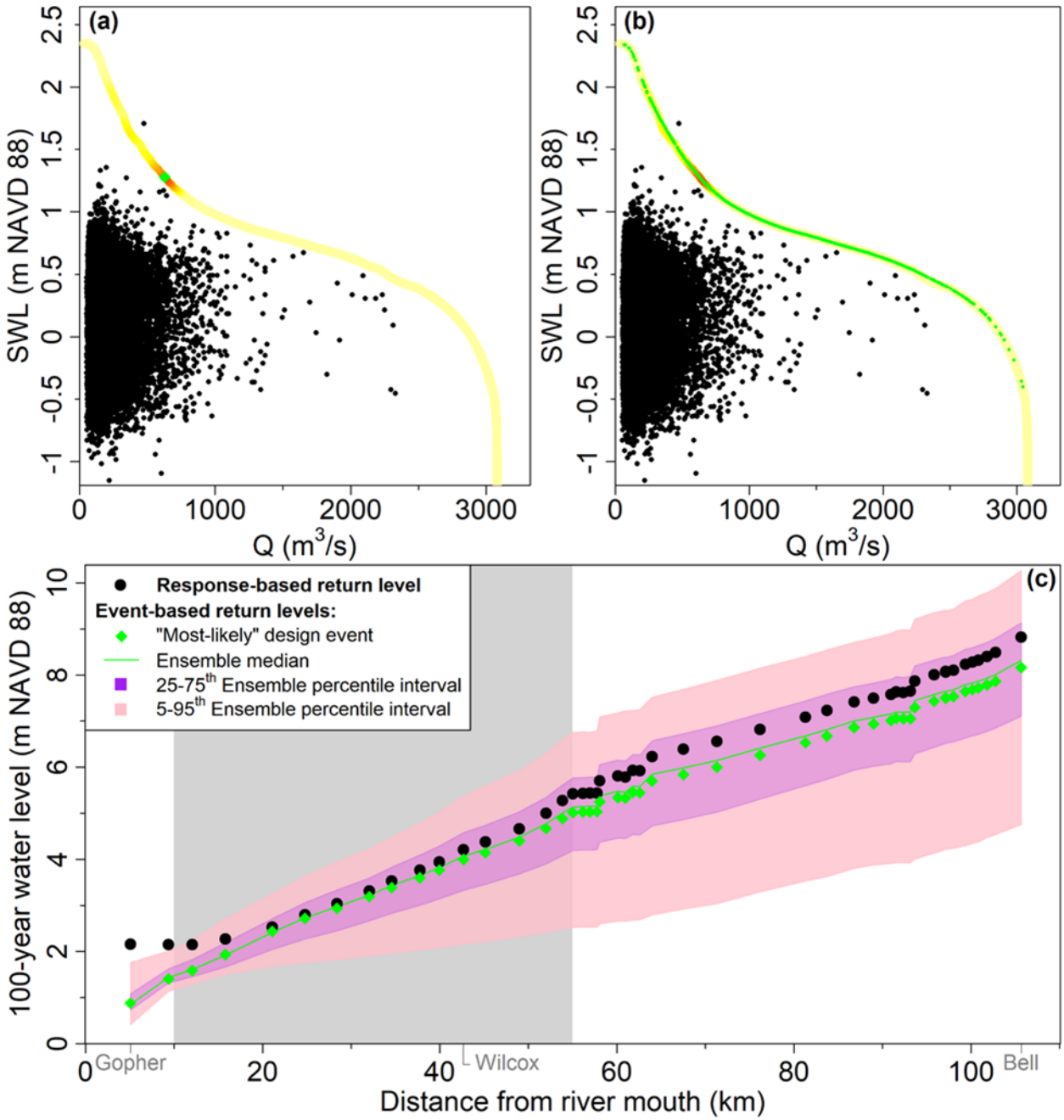

Figure 7: Response-based vs event-based return levels. The 100-year isoline is shown in (a) and (b) with the color contour denoting the relative probability of events on the isoline (hotter colors indicate higher probabilities). In (a) the diamond denotes the "most-likely" design event while the circles in (b) are the ensemble of 1,000 design events. (c) 100-year return levels according to the two approaches with the transition zone shaded in gray.

5 Discussion

The framework proposed in this study derives spatially coherent estimates of return levels along the entire lower course of the river, enabling the exact position of the transition zone to be identified for Q-SWL events of different magnitudes. Despite weak non-statistically significant

correlations in the conditional samples to which the statistical model is fit, the length of the Suwanee River transition zone is found to be far from negligible for all types of conditions investigated. The Suwannee's transition zone is in fact longer than those found on the U.S. West Coast where the dependence between the drivers is far stronger. This contrast in transition zone lengths illustrates the influence of river and catchment characteristics, and highlights the possible threat of compound flooding in localities where it is not usually acknowledged (e.g., places with low dependence between the upstream and downstream flood drivers).

The transition zone identified by the proposed framework for the Suwannee River generally corroborates previous findings. Brown et al. (2016) reported a tidal influence on the ground-surface water interaction at Manatee Springs, approximately 12 km downstream of the Wilcox gauge. McPherson and Hammett (1991) indicated the normal reach of the tide lies between the Manatee Springs and Wilcox gauges. According to Mattson and Rowan (1989), the Wilcox gauge coincides with the head of the tide. Bales et al. (2006) concluded only flows under approximately 450 m^3/s at Wilcox are tidally influenced. The spawning patterns of Suwannee River Gulf sturgeon analyzed over a two-year period imply the head of the tide is approximately between the Wilcox and Bell gauges (Sulak and Clugston, 1998). An analytical tide propagation model fit to near yearlong records at Wilcox and six other gauges farther downstream by Laurel-Castillo and Valle-Levinson (2020), suggest certain harmonics reach even farther upstream. Similarly, a report by The Howard T. Odum Florida Springs Institute (2015) notes that most of the Lower Suwannee River, south of the mouth of the Santa Fe is tidal during periods of low flow due to the river's mild slope. In terms of identifying the transition zone these previous studies suffer several limitations, most notably they are either based on measurements at discrete distances along the river or only analyze a single component of water level (e.g., tide). The adoption of a hybrid framework that accounts for multiple drivers and provides continuous estimates of along-river level negates these shortcomings.

The proposed framework represents a simplification of the flooding process relying on several statistical and physical assumptions. However, the component-wise nature of the framework allows different models to be 'plugged in' to calibrate the assumptions to user-needs for a given study site. For example, a practitioner may wish to employ a different approach in the statistical component. One example is the conditional sampling-copula theory approach, extensively applied in recent studies to identify the potential for compound events (e.g., Wahl et al., 2015; Jane et al., 2022). Presently, the framework assumes no seasonality between discharge and NTR. However, the southeastern U.S. is exposed to several hydrometerological regimes including tropical cyclones, warm season thunderstorm systems, and winter-spring extratropical cyclonic systems (Millar, 1990). Fitting separate models to the different populations of events, by adopting seasonality as a proxy for the hydrometerological conditions, will potentially increase the robustness of the modeling (Villarini and Smith, 2010). Partitioning the data in this way has revealed stronger correlations in the conditional samples (Kim et al., 2022). The rarity of conditions such as tropical cyclones may necessitate the inclusion of water levels from synthetic events propagated through a storm surge model to complement the existing in situ records (Dullaart et al., 2021). The flexibility of the statistical modeling component extends to the inclusion of other drivers that contribute to the flood hazard such as precipitation, waves, or river discharge from multiple tributaries.

More complex data-driven surrogate models such as artificial neural networks (Peters et al., 2006) could seamlessly replace the simple surrogates in the current framework. Alternatively,

integrating lower-fidelity surrogates (Razavi et al., 2012), simplified simulation models which attempt to preserve the processes in the high fidelity numerical model, may increase confidence in the results among practitioners (Bomers et al., 2019). In terms of the hydraulic modeling component, lateral flow variability is typically far more significant in estuarine regions than along a river. If the transition zone is found to start within an estuary, 2D HEC-RAS or an alternate such as DELFT3D-FLOW (Lesser et al., 2004) could be 'plugged in' as a substitute for the 1D HEC-RAS model. In regions where the relative contribution of waves to the downstream ocean level is substantial, hydraulic models can be coupled with wave models (e.g. Kupfer et al., 2022). Adopting rainfall in the statistical modeling component, perhaps because global climate model output is used in the absence of in situ discharge data, may necessitate coupling the hydraulic model with a rainfall-runoff model.

The application of the framework characterizes the present-day compound flood hazard. Future work could include re-applying the framework to account for projected changes in climate and sea level. For instance, by 2100 mean sea level is projected to rise by approximately 2 m at Cedar Key under a high emissions scenario (Sweet et al., 2012). Sea level rise combined with lower freshwater flow, due to increased human extraction in the wider basin or as a result of climate change (e.g. Neupane et al., 2019), may cause the migration of the estuary and hence the transition zone farther inland (e.g., Nelson et al., 2017). The impact of predicted changes in surge height and duration on the flood hazard will potentially be different to, but compounded by, sea level rise (Harrison et al., 2021). In addition to altering the frequency and intensity of the individual drivers, climate change can also alter the dependence between them (e.g., Gori et al., 2022; Wahl et al., 2015), potentially escalating the compound flood hazard including the length of the transition zone.

A surrogate model is not strictly required for the application of the 1D HEC-RAS model in this study, however it plays an important role in ensuring the proposed framework is both flexible and transferable. For rivers with longer transition zones or estuaries with more lateral flow, developing a surrogate model will enable hydraulic models with a greater computational burden, e.g., those covering a larger area or 2D models, to form part of the framework. Considering the impact of different climate change futures, often expressed as a matrix of changes in Q and sea-level rise, potentially involves scaling up the number of model runs by several orders of magnitude. Without a surrogate component, the framework could not be applied to explore different climates futures. Finally, in the event-based approach we calculate the return levels for an ensemble of possible design events, to account for the uncertainty in choosing a single design event. A surrogate model will enable the uncertainty in the response-based return levels to be quantified in an analogous fashion by simulating multiple 10,000 years' worth of events from the statistical model and propagated through the framework.

Although the framework is transferable it may not be applicable at every location due to a lack of data. For instance, the statistical modeling requires overlapping, in situ or numerical riverine and coastal water level records, potentially partitioned to account for seasonality (Couasnon et al., 2022). High resolution digital elevation data is a prerequisite for the numerical modeling, and not available everywhere. The numerical modeling component can explicitly account for modifications to the river channel within the model domain, and can be extended to incorporate unsteady flow conditions and processes which require 2D models. However, accounting for sources of non-stationarity outside of meteorological conditions will likely require modeling additional physical processes, e.g., incorporating land-use changes will likely

necessitate a rainfall-runoff modeling component and switching to rainfall instead of discharge in the statistical modeling (Wu et al., 2021).

Several case studies identified the phase-lag between the principal drivers, storm surge, tide, and rainfall, as a key predictor of flood severity in transition zones (Gori et al., 2020; Harrison et al., 2021). For example, a pulse from the ocean initiated flooding in the St. Johns River during Hurricane Irma; however, peak water levels arose as winds were receding and river discharge increasing (Juarez et al., 2022). The flooding was exacerbated by increases in the magnitude of tides and storm surges in the St. Johns River over the past century, primarily due to channel deepening, with the maximum increases found approximately 20-25 km inland (Talke and Jay, 2020). Currently, the hydraulic modeling part of our framework conservatively assumes daily maximum hourly NTR coincides with peak discharge. Extending the framework to account for phase-lags between the key drivers may yield more accurate estimations of along-river water levels. Over the past 70 years the tidal range has also increased at Cedar Key (Li et al. 2021), however at approximately 0.87 m, it remains relatively small compared with those in other parts of the world. The method we adopted to account for seasonality between NTR and the tide has been successfully applied around the coast of the England where the tidal range is far greater (Gouldby et al. 2017). Given the wide applicability of the framework, another avenue of future work is its implementation in different catchments on the eastern U.S. coast and farther afield to relate the lengths of the transition zones to physical catchment characteristics. This will enable stakeholders (such as state and federal agencies) to prioritize catchments where numerical models able to account for the compound effects between oceanographic and fluvial processes are most urgently required.

6 Conclusions

A transferable framework that combines multivariate statistical methods with hydraulic and surrogate modeling is presented for assessing the compound flood hazard and is demonstrated in the Suwannee River, FL. The statistical modeling part of the framework involves fitting the HT04 model to capture the dependence between Q-NTR. A long synthetic set of events, where at least one of the drivers is extreme, is then simulated from the fitted model. The MDA is applied to select a subset of the synthetic SWL-Q events (after including the tide) to run through the HEC-RAS model, while the remainder are propagated through a surrogate model. An existing HEC-RAS model was modified to only include the river's lower course and shown to perform well during validation. Scattered interpolation proved to be a superior surrogate model to multiple linear regression and radial basis functions. The framework estimated the transition zone of the Suwannee River to be longer than those found in similar studies for the U.S. West Coast (Moftakhari et al., 2019; Serafin et al., 2019). The wider transition zone of the Suwannee is potentially due to the basin's shallower topography and increased ground-surface water interaction both contributing to the catchment's slow response time, along with the existing tidal regime and typical surge characteristics. There is substantial variation in the event-based along-river return levels of the events sampled along the 100-year isoline derived under the "AND" hazard scenario when they are run through the surrogate model; in other words, the ensemble of events which all have a bivariate return period of 100 years lead to a large spread of along-river water levels. This disparity in the return levels highlights a limitation of certain event-based approaches that arise due to the difference in the return period of the response (i.e. along-river levels) and that of the drivers. Nonetheless, in this case study, the

"most-likely" design event on the 100-year isoline leads to very similar return levels as compared to the response-based approach for most of the transition zone.

Acknowledgments

This project is funded, in part, by the US Coastal Research Program (USCRP) as administered by the US Army Corps of Engineers® (USACE), Department of Defense. The content of the information provided in this publication does not necessarily reflect the position or the policy of the government, and no official endorsement should be inferred. The authors acknowledge the USACE and USCRP's support of their effort to strengthen coastal academic programs and address coastal community needs in the United States. T.W. also acknowledges support from the USACE Climate Preparedness and Resilience Community of Practice and Programs and the National Science Foundation under Grant AGS-1929382. The development of the MultiHazard package which was used in the statistical analysis component of the work was funded by the South Florida Water Management District.

Open Research

The still water level data are available from the National Oceanographic and Atmospheric Administration (NOAA) Tides & Currents database (https://tidesandcurrents.noaa.gov/). River discharge data are available through the U.S. Geological Survey (USGS) National Water Information System (https://waterdata.usgs.gov/nwis/rt). Statistical analysis was undertaken in R (R Core Team, 2018) using the MultiHazard package (Jane et al., 2020). The hydraulic modeling component utilized a Hydrologic Engineering Center – River Analysis System (HEC-RAS) model (HEC, 2002) developed by AMEC SRWMD (2013; 2014) available at https://www.mysuwanneeriver.com/DocumentCenter/Index/78.

References

Andrei, A., B. Robert, and B. Erika (2017) Numerical limitations of 1D hydraulic models using MIKE11 or HEC-RAS software - case study of Baraolt River, Romania, IOP Conference Series:

770 Materials Science and Engineering, 245(7), 072010. https://doi.org/10.1088/1757-
771 899X/245/7/072010.
772 AMEC SRWMD (2014) Upper Suwannee River Watershed Redelineation Report.
773 AMEC SRWMD (2013) Lower Suwannee River Watershed Redelination Report.
774 Amidror, I. (2002) Scattered data interpolation methods for electronic imaging systems: a
775 survey, J. Electron. Imaging., 11(2), 157-176. https://doi.org/1017-9909/2002/$15.00
776 Apel, H., B. Merz, and A. H. Thieken (2008). Quantification of uncertainties in flood risk
777 assessments, Int. J. River Basin Manag., 6(2), 149-162.
778 https://doi.org/10.1080/15715124.2008.9635344.
779 Bales, J., S. A. Tomlinson and G. Tillis (2006) Flow and salt transport in the Suwannee River
780 Estuary, Florida, 1999–2000: Analysis of data and three-dimensional simulations (Professional
781 Paper 1656-B). Tallahassee, FL: U.S. Geological Survey.
782 Bass, B., and P. Bedient (2018) Surrogate modeling of joint flood risk across coastal watersheds,
783 J. Hydrol., 558, 159-173. https://doi.org/10.1016/j.jhydrol.2018.01.014.
784 Bender, J., T. Wahl, A. Müller, and J. Jensen (2016) A multivariate design framework for river
785 confluences, Hydrolog. Sci. J., 61(3), 3471-482.
786 https://doi.org/10.1080/02626667.2015.1052816.
787 Benke, A. C. (1990) A perspective on America's vanishing streams, J. North Am. Benthol. Soc.,
788 9, 77–88. https://doi.org/10.2307/1467936
789 Bermúdez, M., L. Cea and J. Puertas (2018) A rapid flood inundation model for hazard mapping
790 based on least squares support vector machine regression, J. Flood Risk Manag., 12, e12522.
791 https://doi.org/10.1111/jfr3.12522

792 Bermúdez, M, L. Cea, and J. Puertas (2019) A rapid flood inundation model for hazard mapping
793 based on least squares support vector machine regression. J Flood Risk Management, 12(Suppl.
794 1):e12522. https://doi.org/10.1111/jfr3.12522.
795 Bevacqua, E., D. Maraun, I. Hobæk Haff, M. Widmann, and M. Vrac (2017) Multivariate
796 statistical modelling of compound events via pair-copula constructions: analysis of floods in
797 Ravenna (Italy), Hydrol. and Earth Sys. Sci., 21, 2701–2723. https://doi.org/10.5194/hess-21-
798 2701-2017.
799 Bevacqua, E., M. I. Vousdoukas, G. Zappa, K. Hodges, T. G. Shepherd, D. L. Maraun,
800 Mentaschi, and L. Feyen (2020) More meteorological events that drive compound coastal
801 flooding are projected under climate change, Commun. Earth Environ., 1, 47.
802 https://doi.org/10.1038/s43247-020-00044-z.
803 Bilskie, M., and S. Hagen (2018) Defining Flood Zone Transitions in Low-Gradient Coastal
804 Regions, Geophys. Res. Lett., 45, 2761–2770. https://doi.org/10.1002/2018GL077524.
805 Boissonnat, J. D., and F. Cazals (2002) Smooth surface reconstruction via natural neighbour
806 interpolation of distance functions, Comput. Geom., 22(1-3), 185-203.
807 https://doi.org/10.1016/S0925-7721(01)00048-7.
808 Bomers, A., R. M. J. Schielen, and S. J. M. H. Hulscher (2019) Application of a lower-fidelity
809 surrogate hydraulic model for historic flood reconstruction, Environ. Model. Softw., 117, 223-
810 236. https://doi.org/10.1016/j.envsoft.2019.03.019.
811 Brown, A. L., C. Young, and J. B. Martin (2016) Groundwater-surface water interactions in the
812 Suwannee River Basin, Fla. Sci., 79(4), 220–238. http://www.jstor.org/stable/44113187.

Camus, P., F. J. Mendez, R. Medina, and A. S. Cofiño (2011a) Analysis of clustering and selection algorithms for the study of multivariate wave climate, Coast. Eng., 58, 453–462, https://doi.org/10.1016/j.coastaleng.2011.02.003.

Camus, P., F. J. Mendez, and R. Medina (2011b) A hybrid efficient method to downscale wave climate to coastal areas, Coast. Eng., 58, 851–862, https://doi.org/10.1016/j.coastaleng.2011.05.007.

Chen, B., D. R. Harp, R. J. Pawar, P. H. Stauffer, H. S. Viswanathan, and R. S. Middleton (2020) Frankenstein's ROMster: Avoiding pitfalls of reduced-order model development, Int. J. Greenh. Gas Control, 93, 102892. https://doi.org/10.1016/j.ijggc.2019.102892.

Coles, S.G., and J. A. Tawn (1991) Modelling extreme multivariate events, J. R. Stat. Soc. Ser. B Methodol., 53 (2), 377–392.

Couasnon, A., A. Sebastian, and O. Morales-Nápoles (2018) A Copula-Based Bayesian Network for Modeling Compound Flood Hazard from Riverine and Coastal Interactions at the Catchment Scale: An Application to the Houston Ship Channel, Texas, Water, 10(9), 1190. https://doi.org/10.3390/w10091190.

Couasnon, A., P. Scussolini, T. V. T. Tran, D. Eilander, S. Muis, H. Wang, et al. (2022) A flood risk framework capturing the seasonality of and dependence between rainfall and sea levels - an application to Ho Chi Minh City, Vietnam, Water Resour. Res., e2021WR030002. https://doi.org/10.1029/2009WR008395.

Didier, D, J. Baudry, P. Bernatchez, et al. (2019) Multihazard simulation for coastal flood mapping: Bathtub versus numerical modelling in an open estuary, Eastern Canada, J. Flood Risk Manag., 12, e12505. https://doi.org/10.1111/jfr3.12505

Dullaart, J. C. M., S. Muis, N. Bloemendaal, M. V. Chertova, A. Couasnon, and C. J. H. Aerts (2021) Accounting for tropical cyclones more than doubles the global population exposed to low-probability coastal flooding, Commun. Earth Environ., 2, 135. https://doi.org/10.1038/s43247-021-00204-9.

Dykstra, S. L., and B. Dzwonkowski (2021) The role of intensifying precipitation on coastal river flooding and compound river-storm surge events, northeast Gulf of Mexico, Water Resour. Res., 57, e2020WR029363. https://doi.org/10.1029/2020WR029363.

Goodell, C. (2014) Breaking the HEC-RAS Code: A User's Guide to Automating HEC-RAS, h2ls, Portland, OR, USA.

Gori, A., N. Lin, and J. Smith (2020) Assessing compound flooding from landfalling tropical cyclones on the North Carolina coast, Water Resour. Res., 56, e2019WR026788. https://doi.org/10.1029/2019WR026788.

Gori, A., N. Lin, D. Xi, and K. Emanuel (2022) Tropical cyclone climatology change greatly exacerbates US extreme rainfall–surge hazard, Nat. Clim. Chang. 12, 171–178. https://doi.org/10.1038/s41558-021-01272-7

Gouldby, B., F. J. Méndez, Y. Guanche, A. Rueda, and R. Mínguez (2014) A methodology for deriving extreme nearshore sea conditions for structural design and flood risk analysis, Coast. Eng., 88, 15-26. http://doi.org/10.1016/j.coastaleng.2014.01.012.

Gouldby, B., D. Wyncoll, M. Panzeri, M. Franklin, T. Hunt, D. Hames, N. Tozer, P. Hawkes, U. Dornbusch, and T. Pullen (2017) Multivariate extreme value modelling of sea conditions around the coast of England. In Proceedings of the Institution of Civil Engineers-Maritime Engineering, 170 (1), 3-20. Thomas Telford Ltd. https://doi.org/10.1680/jmaen.2016.16.

857 Gräler, B, M. van den Berg, S. Vandenberghe, A. Petroselli, S. Grimaldi, B. De Baets, and N.
858 Verhoest (2013) Multivariate Return Periods in Hydrology: a Critical and Practical Review
859 Focusing on Synthetic Design Hydrograph Estimation, Hydrol. Earth Syst. Sci., 17(4), 1281–
860 1296. https://doi.org/10.5194/hess-17-1281-2013.
861 Haigh, I. D., M. Eliot, and C. Pattiaratchi (2011) Global influences of the 18.61 year nodal cycle
862 and 8.85 year cycle of lunar perigee on high tidal levels, J. Geophys. Res. Oceans, 116(C6).
863 https://doi.org/10.1029/2010JC006645.
864 Haigh, I. D., M. P. Wadey, T. Wahl, O. Ozsoy, R. J. Nicholls, J. M. Brown, K. Horsburgh, and
865 B. Gouldby (2016) Spatial and temporal analysis of extreme sea level and storm surge events
866 around the coastline of the UK, Sci. Data, 3(1), 1–14. https://doi.org/10.1038/sdata.2016.107.
867 Harrison, L. M., T. J. Coulthard, P. E. Robins, and M. J. Lewis (2021) Sensitivity of Estuaries to
868 Compound Flooding, Estuaries and Coasts, https://doi.org/10.1007/s12237-021-00996-1
869 HEC-RAS (2002) user's manual available at www.hec.usace.army.mil/software/hec-ras/.
870 Heffernan, J.E., and J. A. Tawn (2004) A conditional approach for multivariate extreme values
871 (with discussion), J. R. Stat. Soc. B., 680 Met., 66(3), 497-546, 2004.
872 https://doi.org/10.1111/j.1467-9868.2004.02050.x.
873 Hicks, F. E., and T. Peacock (2005) Suitability of HEC-RAS for Flood Forecasting, Can. Water
874 Resour. J, 30(2), 159–174. https://doi.org/10.4296/cwrj3002159.
875 Huţanu, E., A. Mihu-Pintilie, A. Urzica, L. E. Paveluc, C. C. Stoleriu, and A. Grozavu (2020)
876 Using 1D HEC-RAS modeling and LiDAR data to improve flood hazard maps' accuracy: A
877 casestudy from Jijia floodplain (NE Romania), Water, 12(6), 1624.
878 https://doi.org/10.3390/w12061624.

Jane, R., L. Cadavid, J. Obeysekera, and T. Wahl (2020) Multivariate statistical modelling of the drivers of compound flood events in South Florida, Nat. Hazards and Earth Sys. Sci., 20, 2681–2699. https://doi.org/10.5194/nhess-20-2681-2020.

Jane, R., T. Wahl, V. M. Santos, S. K. Misra, and K. D. White (2022) Assessing the potential for compound storm surge and extreme river discharge events at the catchment scale with statistical models: sensitivity analysis and recommendations for best-practice, J. Hydrol. Eng., 27(3), 04022001. https://doi.org/10.1061/(ASCE)HE.1943-5584.0002154.

Jhong, B. C., J. H. Wang, and G. F. Lin (2017) An integrated two-stage support vector machine approach to forecast inundation maps during typhoons, J. Hydro., 547, 236–252. https://doi.org/10.1016/j.jhydrol.2017.01.057.

Juarez, B., S. Stockton, K. A. Serafin, and A. Valle-Levinson (2022) Compound flooding in a subtropical estuary caused by Hurricane Irma in 2017, Earth and Space Science Open Archive, 13, 2022, https://doi.org/10.1002/essoar.10511398.1.

Katz, B. G., R. S. DeHan, J. J. Hirten, and J. S. Catches (1997) Interactions Between Ground Water and Surface Water in the Suwannee River Basin, Florida, JAWRA Journal of the American Water Resources Association, 33(6), 1237–1254.

Keef, C., J. A. Tawn, and C. Svensson (2009) Spatial risk assessment for extreme river flows, Appl. Stat., 58, 601-618. https://doi.org/10.1111/j.1467-9876.2009.00672.x.

Kendall, M. G. (1975) Rank Correlation Methods. New York, NY: Oxford University Press.

Kennard, R.W., and L. A. Stone (1969) Computer aided design of experiments, Technometrics, 11 (1), 137–148. https://doi.org/10.1080/00401706.1969.10490666.

Kim, H., G. Villarini, R. Jane, T. Wahl, S. Misra, and A. Michalek (2022) On the generation of high-resolution probabilistic design events capturing the joint occurrence of rainfall and storm surge in coastal basins. Int J Climatol., 1-11. https://doi.org/10.1002/joc.7825.

Kumbier, K., R. C. Carvalho, A. T. Vafeidis, and C. D. Woodroffe (2018) Investigating compound flooding in an estuary using hydrodynamic modelling: a case study from the Shoalhaven River, Australia. Hazards Earth Syst. Sci., 18, 463–477. https://doi.org/10.5194/nhess-18-463-2018.

Kupfer, S., S. Santamaria-Aguilar, L. Van Niekerk, M. Lück-Vogel, and A. Vafeidis, (2022) Investigating the interaction of waves and river discharge during compound flooding at Breede Estuary, South Africa, Nat. Hazards Earth Syst. Sci., 22, 187-205. 10.5194/nhess-22-187-2022

Lan, M., P. Gardoni, R. Luo, J. Zhu and S. Lo (2022) Risk-driven statistical modeling for hurricane-induced compound events: Design event implementation for industrial areas subjected to coastal floods and winds, Ocean Eng., 251, 111-159, https://doi.org/10.1016/j.oceaneng.2022.111159.

Lara J. L., D. Lucio, A. Tomas, B. D. Paolo, and I. J. Losada (2019) High-resolution time-dependent probabilistic assessment of the hydraulic performance for historic coastal structures: application to Luarca Breakwater, Phil. Trans. R. Soc. A, 377: 20190016. http://dx.doi.org/10.1098/rsta.2019.0016.

Laurel-Castillo, J. A., and A. Valle-Levinson (2020) Tidal and subtidal variations in water level produced by ocean-river interactions in a subtropical estuary, J. Geophys. Res. Oceans, 125, e2018JC014116. https://doi.org/10.1029/2018JC014116.

921 Lesser, G. R., J. A. Roelvink, J. A. T. M. van Kester, and G. S. Stelling (2004) Development and
922 validation of a three-dimensional morphological model, Coast. Eng., 51, 883-915.
923 https://doi.org/10.1016/j.coastaleng.2004.07.014.
924 Li, S., T. Wahl, S. A. Talke, D. A. Jay, P. M. Orton, L. Xinghui, G. Wang, and L. Liu (2021)
925 Evolving tides aggravate nuisance flooding along the U.S. coastline, Science Advances, 7(10),
926 eabe2412, 10.1126/sciadv.abe2412.
927 Liem, R. P., C. A. Mader, and J. R. R. A. Martins (2015) Surrogate models and mixtures of
928 experts in aerodynamic performance prediction for aircraft mission analysis, Aerosp. Sci.
929 Technol., 43, 126-151. https://doi.org/10.1016/j.ast.2015.02.019.
930 Lin, G. F.,and L. H. Chen (2004) A non-linear rainfall-runoff model using radial basis function
931 network, J. Hydrol., 289(1-4), 1-8. 10.1016/j.jhydrol.2003.10.015.
932 Liudahl, K., R. L. Weatherspoon, and E. L. Readle (2005) Soil Survey of Dixie County, Florida.
933 United States Department of Agriculture, Natural Resources Conservation Service; in
934 cooperation with the University of Florida Institute for Food and Agricultural Sciences,
935 Washington, D. C.
936 Loveland, M., A. Kiaghadi, C. N. Dawson, H. S. Rifai, S. K. Misra, H. Mosser, and A. Parola
937 (2021) Developing a Modeling Framework to Simulate Compound Flooding: When Storm Surge
938 Interacts With Riverine Flow, Front. Clim., 2, 609610.
939 https://doi.org/10.3389/fclim.2020.609610.
940 Lucey, J. T. D., and T. W. Gallien (2022) Characterizing multivariate coastal flooding events in a
941 semi-arid region: the implications of copula choice, sampling, and infrastructure, Nat. Hazards
942 Earth Syst. Sci., 22, 2145–2167. https://doi.org/10.5194/nhess-22-2145-2022.

943 Majdisova, Z., and V. Skala (2017) Radial basis function approximations: comparison and
944 applications, Appl. Math. Model., 51, 728-743. https://doi.org/10.1016/j.apm.2017.07.033.
945 Malde, S., D. Wyncoll, J. Oakley, N. Tozer, and B. Gouldby (2016) Applying emulators for
946 improved flood risk analysis, In: E3S Web Conf, vol. 7. pp. 04002. https://doi.org/10.
947 1051/e3sconf/20160704002.
948 Mann, H. B. (1945) Nonparametric tests against trend, Econometrica 13, 245–259.
949 https://doi.org/10.2307/1907187.
950 Mattson, R. A., and M. E. Rowan (1989) The Suwannee River estuary: An overview and
951 research and management needs, in Davis, F.E., ed., Water: Laws and Management: Betheseda,
952 Md., American Water Resources Association, p. 14B17–14B31.
953 McPherson, B. F., and K. M. Hammett (1991) Tidal Rivers of Florida, Pp. 31-46 IN: R. J.
954 Livingston (ed.), The Rivers of Florida, Ecological Studies, Vol. 83. Springer-Verlag, New
955 York, NY.
956 Medellín, G., J. A. Brinkkemper, A. Torres-Freyermuth, C. M. Appendini, E. T. Mendoza, and
957 P. Salles (2016) Run-up parameterization and beach vulnerability assessment on a barrier island:
958 a downscaling approach, Nat. Hazards Earth Syst. Sci., 16, 167–180,
959 https://doi.org/10.5194/nhess-16-167-2016.
960 Moftakhari, H., J. E. Schubert, A. AghaKouchak, R. A. Matthew, and B. F. Sanders (2019)
961 Linking statistical and hydrodynamic modeling for compound flood hazard assessment in tidal
962 channels and estuaries, Adv. Water Resour., 128, 28–38.
963 https://doi.org/10.1016/j.advwatres.2019.04.009.
964 Miller, A. J. (1990) Flood hydrology and geomorphic effectiveness in the central Appalachians,
965 Earth Surf. Process. Landf., 15, 119–134. https://doi.org/10.1002/esp.3290150203.

966 Mossaa J., and J. Konwinski (1998) Thalweg variability at bridges along a large karst river: the
967 Suwannee River, Florida. Eng. Geol., 49(1), 15-30. https://doi.org/10.1016/S0013-
968 7952(97)00034-3.
969 Muñoz, D. F., H. Moftakhari, and H. Moradkhani (2020) Compound effects of flood drivers and
970 wetland elevation correction on coastal flood hazard assessment, Water Resour. Res., 56,
971 e2020WR027544. https://doi.org/10.1029/2020WR027544.
972 Nadal-Caraballo, N. C., J. A. Melby, and V. M. Gonzalez (2016). Statistical Analysis of
973 Historical Extreme Water Levels for the U.S. North Atlantic Coast Using Monte Carlo Life-
974 Cycle Simulation, J. Coast. Res., 317, 35–45. https://doi.org/10.2112/jcoastres-d-15-00031.1
975 Nelson, N. G., S. Ward, and D. Ward (2017) Implications of altered freshwater flows on
976 estuarine fish and shellfish: a case study of the Lower Suwannee River, White paper prepared for
977 the Florida Climate Institute, UF Levin College of Law, and UF/IFAS Nature Coast Biological
978 Station.
979 Neupane, R. P., D. L. Ficklin, J. H. Knouft, N. Ehsani, and R. Cibin (2019) Hydrologic
980 responses to projected climate change in ecologically diverse watersheds of the Gulf Coast,
981 United States. Int. J. Climatol., 39, 2227–2243. https://doi.org/10.1002/joc.5947
982 Nasr, A. A., T. Wahl, M. M. Rashid, P. Camus, and I. D. Haigh (2021) Assessing the
983 dependence structure between oceanographic, fluvial, and pluvial flooding drivers along the
984 United States coastline, Hydrol. Earth Syst. Sci., 25, 6203–6222. https://doi.org/10.5194/hess-25-
985 6203-2021.
986 van Ormondt, M., D. Roelvink, and A. P van Dongeren (2021) A Model-Derived Empirical
987 Formulation for Wave Run-Up on Naturally Sloping Beaches, J. Mar. Sci. Eng., 9(11), 1185.
988 https://doi.org/10.3390/jmse9111185.

Parker, J. A., R. V. Kenyon, and D. E. Troxel (1983) Comparison of interpolating methods for image resampling, IEEE Transactions on medical imaging, 2(1), 31-39. https://doi.org/10.1109/TMI.1983.4307610.

Parker, K., P. K. Ruggiero, K. Serafin, and D. Hill (2019) Emulation as an Approach for Rapid Estuarine Modeling, Coast. Eng., 150, 79–93. https://doi.org/10.1016/j.coastaleng.2019.03.004.

Pathan, A. I., and P. G. Agnihotri (2020) Application of new HEC-RAS version 5 for 1D hydrodynamic flood modeling with special reference through geospatial techniques: A case of River Purna at Navsari, Gujarat, India, Model. Earth Syst. Environ., 1–12. https://doi.org/10.1007/s40808-020-00961-0.

Pawlowicz, R., B. Beardsley and S. Lentz (2002) Classical tidal harmonic analysis including error estimates in MATLAB using T_TIDE, Comput. and Geosci., 28(8), 929–937. https://doi.org/10.1016/S0098-3004(02)00013-4

Pettitt, A. N. (1979) A non-parametric approach to the change-point problem, J. R. Stat. Soc., Ser. C, 28(2), 126–135. https://doi.org/10.2307/2346729.

Peters, R., G. Schmitz, and J. Cullmann (2006) Flood routing modelling with Artificial Neural Networks, Adv. Geosci.., 9, 131–136. https://doi.org/10.5194/adgeo-9-131-2006.

Pfahl, S., and H. Wernli (2012) Quantifying the Relevance of Cyclones for Precipitation Extremes, J. Clim., 25(19), 6770-6780. https://doi.org/10.1175/JCLI-D-11-00705.1.

R Core Team (2018) R: A Language and Environment for Statistical Computing. R Found. for Stat. Comp., Vienna: Austria, https://www.R-project.org/

Razavi, S., B. A. Tolson, and D. H. Burn (2012) Review of surrogate modeling in water resources, Water Resour. Res., 48, W07401. https://doi.org/10.1029/2011WR011527

1011 Robinson, T. D., Eldred, M. S., Willcox, K. E., Haimes, R., (2008) Surrogate-based optimization
1012 using multifidelity models with variable parameterization and corrected space mapping, AIAA J.
1013 46(11), 2814–2822. https://doi.org/10.2514/1.36043.
1014 Rohmer, J., and D. Idier (2012) A meta-modelling strategy to identify the critical offshore
1015 conditions for coastal flooding, Nat. Hazards Earth Syst. Sci., 12, 2943-2955.
1016 https://doi.org/10.5194/nhess-12-2943-2012.
1017 Rueda, A., B. Gouldby, F. J. Mendez, A. Tomas, I. J. Losada, J. L. Lara, and P. Diaz-Simal
1018 (2016) The use of wave propagation and reduced complexity inundation models and metamodels
1019 for coastal flood risk assessment, J Flood Risk Manag., 9, 390–401.
1020 https://doi.org/10.1111/jfr3.12204.
1021 Sacks, J., W. J. Welch, J. S. B. Mitchell, P. W. Henry, T. J. Mitchell, and H. P. Wynn (1989)
1022 Design and Experiments of Computer Experiments, Stat. Sci., 4 (4), 409–423.
1023 https://doi.org/10.1214/ss/1177012413.
1024 Saleh, F., V. Ramaswamy, Y. Wang, N. Georgas, A. Blumberg, and J. Pullen (2017) A multi-
1025 scale ensemble-based framework for forecasting compound coastal-riverine flooding: The
1026 Hackensack-Passaic watershed and Newark Bay, Adv. Water Resour., 110, 371–386.
1027 https://doi.org/10.1016/j.advwatres.2017.10.026.
1028 Salvadori, G., C. De Michele, and F. Durante (2011) On the return period and design in a
1029 multivariate framework, Hydrol. Earth Syst. Sci., 15(11), 3293-3305.
1030 https://doi.org/10.5194/hess-15-3293-2011.
1031 Salvadori, G., F. Durante, C. De Michele, M. Bernardi, and L. Petrella (2016) A multivariate
1032 copula-based framework for dealing with hazard scenarios and failure probabilities, Water
1033 Resour. Res., 52, 3701–3721, http://doi.org/10.1002/2015WR017225.

1034 Santiago-Collazo, F. L., M. V. Bilskie, and S. C. Hagen (2019) A comprehensive review of
1035 compound inundation models in low-gradient coastal watersheds, Environ. Model. Softw., 119,
1036 166– 181. https://doi.org/10.1016/j.envsoft.2019.06.002.
1037 Santos, V. M., T. Wahl, J. W. Long, D. L. Passeri, and N. G. Plant (2019) Combining numerical
1038 and statistical models to predict storm-induced dune erosion, J. Geophys. Res. Earth Surf., 124,
1039 1817–1834. https://doi.org/10.1029/2019JF005016.
1040 Santos, V. M., T. Wahl, R. Jane, S. K. Misra, and K. D. White (2021a) Assessing compound
1041 flooding potential with multivariate statistical models in a complex estuarine system under data
1042 constraints, J. Flood Risk Manage., 14(4), e12749. https://doi.org/10.1111/jfr3.12749
1043 Santos, V. M., M. Casas-Prat, B. Poschlod, E. Ragno, B. van den Hurk, Z. Hao, T. Kalmár, L.
1044 Zhu, and H. Najafi (2021b) Statistical modelling and climate variability of compound surge and
1045 precipitation events in a managed water system: a case study in the Netherlands, Hydrol. and
1046 Earth Sys. Sci., 25(6), 3595– 3615. https://doi.org/10.5194/hess-25-3595-2021.
1047 Seavey, J. R., W. E. Pine III, P. Frederick, L. Sturmer, and M. Berrigan (2011) Decadal changes
1048 in oyster reefs in the Big Bend of Florida's Gulf Coast, Ecosphere, 2(10), 114.
1049 https://doi.org/10.1890/ES11-00205.1.
1050 Serinaldi, F. (2015) Dismissing return periods! Stoch. Environmental Res. Risk A., 29(4), 1179–
1051 1189. https://doi.org/10.1007/s00477-014-0916-1.
1052 Serafin, K. A., P. Ruggiero, K. Parker, and D. F. Hill (2019) What's streamflow got to do with it?
1053 A probabilistic simulation of the competing oceanographic and fluvial processes driving extreme
1054 along-river water levels, Nat. Hazards Earth Sys. Sci,. 19(7), 1415-1431.
1055 https://doi.org/10.5194/nhess-2018-347.

1056 Silva-Araya, W., F. Santiago-Collazo, J. Gonzalez-Lopez, and J. Maldonado-Maldonado (2018)
1057 Dynamic modeling of surface runoff and storm surge during hurricane and tropical storm events,
1058 Hydrol., 5, 13. https://doi.org/10.3390/hydrology5010013.
1059 Smith, R. L., and I. Weissman (1994) Estimating the extremal index. J. R. Stat. Soc. Ser. B
1060 56(3), 515–528.
1061 Soleymani, S. A., Goudarzi, S., Anisi, M. H., Hassan, W. H., Idris, M. Y. I., Shamshirband, S.,
1062 and I. Ahmedy (2016) A novel method to water level prediction using RBF and FFA, Water Res.
1063 Manage., 30(9), 3265-3283. https://doi.org/10.1007/s11269-016-1347-1.
1064 SRWMD, (2014) https://www.mysuwanneeriver.com/DocumentCenter/Index/78
1065 Sulak, K. J. and J. P. Clugston (1998) Early Life History Stages of Gulf Sturgeon in the
1066 Suwannee River, Florida, Trans. Am. Fish. Soc., 127(5), 758-771.
1067 https://doi.org/10.1577/1548-8659(1998)127<0758:ELHSOG>2.0.CO;2
1068 Sweet, W.V., B.D. Hamlington, R.E. Kopp, C.P. Weaver, P.L. Barnard, D. Bekaert, W. Brooks,
1069 M. Craghan, G. Dusek, T. Frederikse, G. Garner, A.S. Genz, J.P. Krasting, E. Larour, D. Marcy,
1070 J.J. Marra, J. Obeysekera, M. Osler, M. Pendleton, D. Roman, L. Schmied, W. Veatch, K.D.
1071 White, and C. Zuzak (2022) Global and Regional Sea Level Rise Scenarios for the United States:
1072 Updated Mean Projections and Extreme Water Level Probabilities Along U.S. Coastlines.
1073 NOAA Technical Report NOS 01. National Oceanic and Atmospheric Administration, National
1074 Ocean Service, Silver Spring, MD, 111 pp.
1075 https://oceanservice.noaa.gov/hazards/sealevelrise/noaa-nostechrpt01-global-regional-SLR-
1076 scenarios-US.pdf
1077 Talke, S. A. and D. A. Jay (2020) Changing tides: The role of natural and anthropogenic factors,
1078 Annu. Rev. Mar. Sci. 12, 121–151. https://doi.org/10.1146/annurev-marine-010419-010727.

1079 The Howard T. Oden Florida Springs Institute (2015) Lower Suwannee River
1080 Springs Restoration Plan. https://floridaspringsinstitute.org/wp-content/uploads/2018/07/Lower-
1081 Suwannee-River-Springs-Restoration-Action-Plan-final.pdf
1082 Torres, J. M., B. Bass, N. Irza, Z. Fang, J. Proft, C. Dawson, et al. (2015) Characterizing the
1083 hydraulic interactions of hurricane storm surge and rainfall-runoff for the Houston-Galveston
1084 region, Coast. Eng., 106, 7-19. https://doi.org/10.1016/j. coastaleng.2015.09.004.
1085 Valle-Levinson, A. (2012) Impact of record flooding of a subtropical river on estuary/ocean
1086 exchange, Ocean Dynamics, 62, 77–85. https://doi.org/10.1007/s10236-011-0491-7.
1087 Valle-Levinson, A., M. Olabarrieta and L. Heilman (2020) Compound flooding in Houston-
1088 Galveston Bay during Hurricane Harvey, Sci. Total Environ., 747, 141272.
1089 https://doi.org/10.1016/j.scitotenv.2020.141272.
1090 Villarini, G., and J. A. Smith (2010) Flood peak distributions for the eastern United States, Water
1091 Resour. Res., 46(6), W06504. https://doi.org/10.1029/2009WR008395.
1092 Wahl, T., S. Jain, J. Bender, S. D. Meyers, and M. E. Luther (2015) Increasing risk of compound
1093 flooding from storm surge and rainfall for major US cities, Nat. Clim. Change, 5(12), 1093–
1094 1097. https://doi.org/10.1038/nclimate2736.
1095 Willett, P. (1999) Dissimilarity-Based Algorithms for Selecting Structurally Diverse Sets of
1096 Compounds, J. of Comp. Biol., 6, 447-457. https://doi.org/10.1089/106652799318382
1097 Wu, W., S. Westra, and M. Leonard (2021) Estimating the probability of compound floods in
1098 estuarine regions, Hydrol. Earth Syst. Sci., 25, 2821–2841. https://doi.org/10.5194/hess-25-2821-
1099 2021, 2021.

1100 Wyncoll, D., and B. Gouldby (2015) Integrating a multivariate extreme value method within a
1101 system flood risk analysis model, J. Flood Risk Manage., 8, 145-160.
1102 https://doi.org/10.1111/jfr3.12069.
1103 Yi, X. (2011) A dam break analysis using HEC-RAS, Water Resour. Prot., 3(6), 370-379.
1104 https://doi.org/10.4236/jwarp.2011.36047.
1105 Zahura, F. T., J. L. Goodall, J. M. Sadler, Y. Shen, M. M. Morsy, and M. Behl (2020) Training
1106 machine learning surrogate models from a high-fidelity physics-based model: Application for
1107 real-time street-scale flood prediction in an urban coastal community, Water Resour. Res., 56,
1108 e2019WR027038. https://doi.org/10.1029/2019WR027038.
1109 Zheng, F., S. Westra, M. Leonard, and S. A. Sisson. (2014) Modeling dependence between
1110 extreme rainfall and storm surge to estimate coastal flooding risk, Water Resour. Res., 50(3),
1111 2050–2071. https://doi.org/10.1002/2013WR014616.